

**UNIVERSIDADE ESTADUAL PAULISTA “JÚLIO DE MESQUITA FILHO”
FACULDADE DE ENGENHARIA DE ILHA SOLTEIRA**

VITOR CESAR NOGUEIRA MATTOS

**PARAMETRIC OPTIMIZATION TO DESIGN A HIGH-PERFORMANCE
VANELESS-DIFFUSER FOR SCO_2 CENTRIFUGAL COMPRESSOR**

Ilha Solteira

2022

PROGRAMA DE PÓS-GRADUAÇÃO EM ENGENHARIA MECÂNICA

**Parametric Optimization to Design a High-Performance
Vaneless-Diffuser for sCO₂ Centrifugal Compressor**

Vitor Cesar Nogueira Mattos

Advisor: Prof. Dr. Leandro Oliveira Salviano

Dissertation presented to the College of Engineering – UNESP – Campus at Ilha Solteira, as part of the requirements for obtaining the Master's degree in Mechanical Engineering.

Field of Knowledge: Thermal Sciences.

Ilha Solteira – SP

August/2022

FICHA CATALOGRÁFICA

Desenvolvido pelo Serviço Técnico de Biblioteca e Documentação

M444p Mattos, Vitor Cesar Nogueira.
Parametric optimization to design a high-performance vaneless-diffuser for sCO₂ centrifugal compressor / Vitor Cesar Nogueira Mattos. -- Ilha Solteira: [s.n.], 2022
62 f. : il.

Dissertação (mestrado) - Universidade Estadual Paulista. Faculdade de Engenharia de Ilha Solteira. Área de conhecimento: Ciências Térmicas, 2022

Orientador: Leandro Oliveira Salviano
Inclui bibliografia

1. sCO₂ centrifugal compressor. 2. Optimization. 3. Vaneless-diffuser. 4. CFD.

Raiane da Silva Santos
Raiane da Silva Santos

CERTIFICADO DE APROVAÇÃO

TÍTULO DA DISSERTAÇÃO: PARAMETRIC OPTIMIZATION TO DESIGN A HIGH-PERFORMANCE VANELESS-DIFFUSER FOR S-CO₂ CENTRIFUGAL COMPRESSOR

AUTOR: VITOR CESAR NOGUEIRA MATTOS

ORIENTADOR: LEANDRO OLIVEIRA SALVIANO

Aprovado como parte das exigências para obtenção do Título de Mestre em ENGENHARIA MECÂNICA, área: Ciências Térmicas pela Comissão Examinadora:

Prof. Dr. LEANDRO OLIVEIRA SALVIANO (Participação Virtual) 
Departamento de Engenharia Mecânica / Faculdade de Engenharia de Ilha Solteira - UNESP

Prof. Dr. ALUISIO VIAIS PANTALEÃO (Participação Virtual) 
Departamento de Engenharia Mecânica / Faculdade de Engenharia de Ilha Solteira - UNESP

Prof. Dr. FÁBIO SALTARA (Participação Virtual) 
Departamento de engenharia mecânica / Universidade de São Paulo - Escola Politécnica

Ilha Solteira, 02 de setembro de 2022

ACKNOWLEDGEMENTS

This dissertation was made with the collaboration and support of several personals, so it would be a mistake not to thank them and give the necessary recognition to those who made this moment possible.

First of all, I would like to thank my parents, Maria Madalena and Marcus Cesar, for all the support and help and also for believing in me throughout this journey.

I also thank Catharina, not only for being my life partner and best friend but also for teaching me so many things, including scientific writing and methodology.

To the friends of the republic, who not only shared good times but also supported and motivated me in the most complicated moments.

Finally, I thank Professor Leandro and laboratory colleagues for believing in my potential and showing me the paths of research in thermal sciences.

ABSTRACT

Supercritical carbon-dioxide centrifugal compressors are machines with high potential for use in power generation plants and in the oil industry as it achieves high thermal efficiency in the Brayton cycle and assist in oil production through the capture and storage of CO₂ by the EOR (Enhanced Oil Recovery) method. In this regard, to increase the performance of these machines, a three-dimensional numerical simulation (CFD) coupled with an optimization method is investigated. As well known, one-dimensional modeling for vaneless-diffuser designs is not able to predict all important flow phenomena due to several geometric parameters. Therefore, the present work aims to use the methodology optimization-surrogate coupled with CFD to optimize nine geometric input variables related to a vaneless-diffuser channel to identify the influence of each parameter on the turbomachinery performance and its sources of loss. Three different objective functions are submitted to single-optimization: Maximize total-to-total polytropic efficiency, minimize total pressure loss coefficient or maximize static pressure recovery coefficient. A preliminary geometry is created using Ansys Vista CCD for the impeller and the vaneless-diffuser is modeled as a channel of parallel plates. The sensitivity analysis is conducted using the Morris Elementary Effects method and SS-ANOVA through the response surface generated by Gaussian Process regression. The optimization procedure is fulfilled by the NSGA-II method. The main conclusions indicate that the optimized geometries increased by 2.9% the total-to-total polytropic efficiency, reduced by 24.0% the total pressure loss coefficient and increased by 11.4% the static pressure recovery coefficient at the design-point operational condition. Moreover, the optimal configuration found by the optimization procedure remains with higher performance even operating at the off-design point. The strategy adopted in the present work through a combination of one-dimensional turbomachinery design with three-dimensional parametric sensitivity analysis and CFD-optimization of a vaneless-diffusers is a powerful tool for sizing high-performance equipment.

Keywords: sCO₂ centrifugal compressor, optimization, vaneless-diffuser, CFD.

RESUMO

Os compressores centrífugos supercríticos de dióxido de carbono são máquinas com alto potencial para uso em usinas de geração de energia e na indústria de petróleo, pois atingem alta eficiência térmica no ciclo Brayton e auxiliam na produção de óleo por meio da captura e armazenamento de CO₂ pelo EOR (Enhanced Oil método de recuperação). Nesse sentido, para aumentar o desempenho dessas máquinas, uma simulação numérica tridimensional (CFD) acoplada ao método de otimização é investigada. Como se sabe, a modelagem unidimensional para projetos de difusores sem palhetas não é capaz de prever todos os fenômenos de fluxo importantes devido a vários parâmetros geométricos. Portanto, o presente trabalho tem como objetivo utilizar a metodologia otimização-substituta acoplada ao CFD para otimizar nove variáveis de entrada geométricas relacionadas a um canal difusor sem palhetas para identificar a influência de cada parâmetro no desempenho da turbomáquina e suas fontes de perda. Três funções objetivo diferentes são submetidas à otimização simples: Maximizar a eficiência politrópica total a total, minimizar o coeficiente de perda de pressão total ou maximizar o coeficiente de recuperação de pressão estática. Uma geometria preliminar é criada usando Ansys Vista CCD para o impulsor e o difusor sem palhetas é modelado como um canal de placas paralelas. A análise de sensibilidade é realizada utilizando o método Morris Elementary Effects e SS-ANOVA através da superfície de resposta gerada pela regressão do Processo Gaussiano. O procedimento de otimização é realizado pelo método NSGA-II. As principais conclusões indicam que as geometrias otimizadas aumentaram em 2,9% a eficiência politrópica total a total, reduziram em 24,0% o coeficiente de perda de pressão total e aumentaram em 11,4% o coeficiente de recuperação de pressão estática na condição operacional do ponto de projeto. Além disso, a configuração ótima encontrada pelo procedimento de otimização permanece com desempenho superior mesmo na operação fora do projeto. A estratégia adotada no presente trabalho através da combinação de projeto unidimensional de turbomáquinas com análise de sensibilidade paramétrica tridimensional e otimização CFD de um difusor sem pás é uma ferramenta poderosa para dimensionar equipamentos de alto desempenho.

Palavras-chave: compressor centrífugo de sCO₂, otimização, vaneless-diffuser, CFD.

LIST OF FIGURES

Fig. 1 Schematic of a centrifugal compressor.	12
Fig. 2 Typical diffusers: (a) vaneless diffuser, (b) vaned diffuser.	13
Fig. 3 Typical vaned diffuser geometries: (a) cascade, (b) channel, (c) low-solidity, (d) low-solidity with plate vanes.	13
Fig. 4 Different types of vaneless diffusers.	14
Fig. 5 Original and optimized geometry of a vaneless diffuser channel.	15
Fig. 6 Pressure ratio (Ψ) and adiabatic efficiency (η) comparison between optimized (continuous line) and base geometries (dashed lines) in relation to flow coefficient (ϕ).....	16
Fig. 7 Comparison between performance parameters.	17
Fig. 8 Performance analysis.	18
Fig. 9 Original and optimized performance parameters.	19
Fig. 10 Methodology flowchart.	21
Fig. 11 Computational domain with main components and boundary conditions indicated. ..	23
Fig. 12 Geometrical parameters for optimization.....	25
Fig. 13 Solution method of ANSYS CFX for steady-state problems.....	29
Fig. 14. Meshes used in the analysis: (a) coarse, (b) medium, (c) fine.	32
Fig. 15. Y-plus distribution in the domain to ensure turbulence quality criteria.....	33
Fig. 16 Comparison between surrogate methods.	36
Fig. 17 Non-dominated fronts.	37
Fig. 18 Sorting algorithm.	38
Fig. 19 Elementary effects for polytropic efficiency.....	40
Fig. 20 Elementary effects for Polytropic Efficiency.....	40
Fig. 21 Elementary effects for static pressure recovery.	41
Fig. 22 Elementary effects for Polytropic Efficiency.....	41
Fig. 23 Convergence analysis of Morris method for polytropic efficiency.....	42
Fig. 24 Convergence analysis of Morris method for static pressure recovery.	43
Fig. 25 Convergence analysis of Morris method for pressure ratio.	43
Fig. 26 Convergence analysis of Morris method for total pressure loss.	44
Fig. 27 Contribution indices from SS-ANOVA analysis for polytropic efficiency.	45
Fig. 28 Contribution indices from SS-ANOVA analysis for static pressure recovery.....	45

Fig. 29 Contribution indices from SS-ANOVA analysis for pressure ratio.....	46
Fig. 30 Contribution indices from SS-ANOVA analysis for pressure loss.....	46
Fig. 31 Performance behavior along of the channel length.....	48
Fig. 32 Optimal parameters for polytropic efficiency.....	49
Fig. 33 Optimal parameters for static pressure recovery.....	49
Fig. 34 Optimal parameters for total pressure loss.....	50
Fig. 35 Meridional shape of vaneless diffuser geometries.....	50
Fig. 36 Behavior of the diffuser meridional velocity along the streamwise.....	51
Fig. 37 Streamlines of meridional velocity in (a) baseline, (b) t-t polytropic efficiency optimized and (c) static pressure recovery coefficient optimized geometries.....	52
Fig. 38 Entropy as a function of streamwise.....	53
Fig. 39 Total pressure as a function of streamwise.....	54
Fig. 40 Static pressure as a function of streamwise.....	54
Fig. 41 Shear strain rate contours of (a) baseline geometry, (b) optimal polytropic efficiency and (c) optimal static pressure recovery coefficient.....	55
Fig. 42 Compressor performance in the design Speedline (12.500 RPM).....	56

LIST OF TABLES

Table 1 Geometrical parameters and boundary conditions.	23
Table 2 Variables range definition.	26
Table 3 Grid independence analysis and numerical validation.	31
Table 4 Baseline and optimized geometries.	47

TABLE OF CONTENTS

1.	INTRODUCTION	10
2.	LITERATURE REVIEW	12
3.	METHODOLOGY	21
3.1	GEOMETRY AND BOUNDARY CONDITIONS.....	22
3.2	DISCRETIZATION AND SOLUTION.....	26
3.3	VOLUTE PERFORMANCE.....	30
3.4	GRID ANALYSIS AND NUMERICAL VALIDATION.....	31
3.5	SENSITIVITY ANALYSIS.....	34
3.6	SURROGATE MODEL.....	35
3.7	OPTIMIZATION.....	36
4.	RESULTS AND DISCUSSIONS	39
4.1	SEQUENTIAL SENSITIVITY ANALYSIS.....	39
4.2	OPTIMIZATION.....	47
5.	CONCLUSIONS	57
	REFERENCES	59

1. INTRODUCTION

High-speed centrifugal compressors are rotating machines present in several industrial applications, such as refrigeration, air-conditioning, power generation and automotive turbochargers. More specifically, sCO₂ centrifugal compressors have great potential for application in the oil industry as they can be used to inject supercritical carbon dioxide into underground basins, through a process called CO₂-EOR (Enhanced Oil Recovery), which helps to produce additional oil and remove the pollutant from the atmosphere (GODEC et al., 2011). Godec et al. (2011) estimate that the world has the potential to produce around 470 billion barrels of oil and store 140 gigatons of carbon dioxide using this technique. In addition, supercritical carbon dioxide centrifugal compressors are machines of great interest in the area of electric energy production through the Brayton cycle due to their liquid-like thermodynamic behavior at low temperatures which makes the thermal efficiency increase and the emission of polluting gases decrease (“Technology Assessments”, 2015).

Designing high-performance turbomachinery can be an extremely hard and necessary task due to complex flow conditions like recirculation, adverse pressure gradients and jet-wake patterns (DENTON, 1993) and the high energy potential that can be consumed. Also, to extract the highest possible performance from a stage, it is necessary to properly size the diffuser, a component responsible for recovering static pressure through the kinetic energy obtained in the impeller. In general, the design of this part relies on experimental data, meanline and streamline codes (AUNGIER, 2000) and engineers’ experience.

Describing the complex fluid dynamic behaviors is the object of several papers. Dean & Senoo (1960), Eckardt (1975) and Pinarbasi & Johnson (1995) have characterized and created mathematical models to describe the complex fluid dynamic behaviors such as transient jet-wake pattern, diffusivity and pressure loss in the rotor-stator interaction, which is highly time-dependent, especially within vaneless diffusers. However, this is still based on experimental data and it is extremely dependent on the impeller and diffuser geometries. Hence, due to the increase in computing power over time, Lee et al. (2000), Turunen-Saaresti (2004), and Shaaban (2015) presented more modern alternatives with the application of an optimization method coupled to numerical simulations using Reynolds Average Navier-Stokes (RANS) equations which allows obtaining high-performance impellers and radial diffusers starting from random or pre-existing geometries. However, optimization processes

are still computationally expensive, especially for high-complexity models with many geometric variables, such as compressors.

Therefore, Kim et al. (2010), Sugimura et al. (2012) and He & Zheng (2017). Mojaddam & Pullen (2019) and Salviano et al. (2021) added sensitivity analysis to classify and eliminate variables that do not significantly change the parameters of interest and response surface methods to optimization to transform the complex 3D RANS model into a simple mathematical expression that relates geometric inputs to performance outputs aiming to reduce the computational cost.

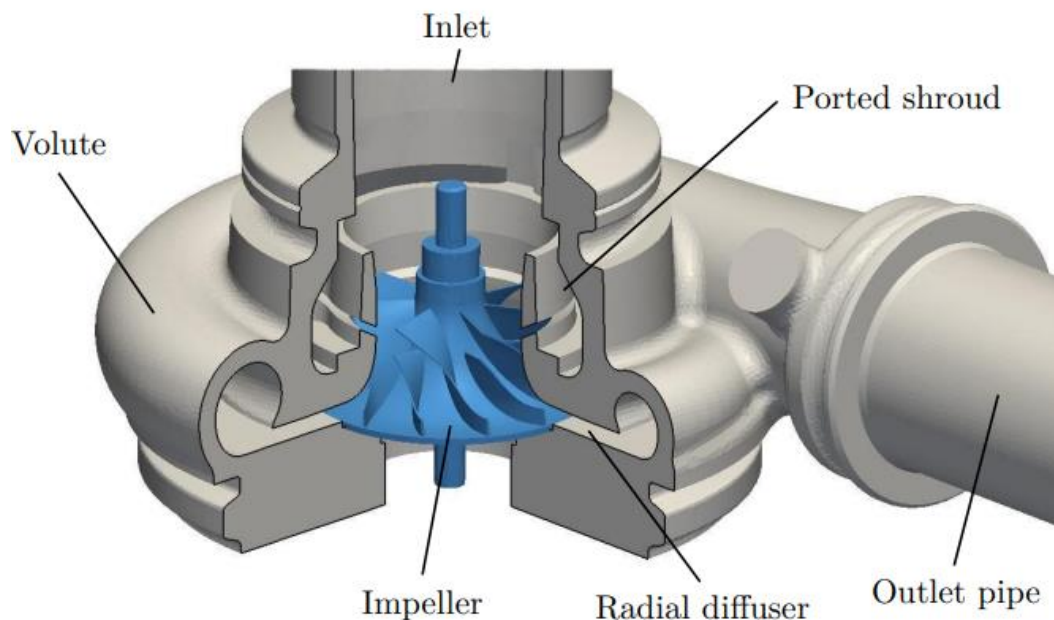
Despite the methodology focused on reducing computational effort adopted by the last works, none of them specifically addressed the impact of the diffuser in their analyses. Moreover, most use optimization as a method to improve an already used geometry and not to design it. Also, the application of such methods to supercritical carbon dioxide compressors is quite new.

Therefore, the present work aims to design a high-efficiency machine through the optimization-surrogate methodology, to reduce the computational effort, coupled to Computational Fluid Dynamics (CFD) by varying nine geometric inputs of a vaneless diffuser channel of supercritical carbon dioxide centrifugal compressor and identify the influence of each parameter on the performance and sources of loss. Three different objective functions are considered: maximize total-to-total polytropic efficiency, minimize total pressure loss coefficient or maximize static pressure recovery coefficient. The baseline geometry of the vaneless-diffuser is built without any mathematical model to demonstrate the power and robustness of the present methodology to find optimal equipment, which is extremely complex through one-dimensional methods. In addition, the method makes it possible to increase static pressure recovery and machine efficiency without the need for blades at the diffuser and, consequently, without reducing the surge margin.

2. LITERATURE REVIEW

In general, a single-stage centrifugal compressor, indicated in Fig. 1, is divided into three main parts: impeller, responsible for increasing the dynamic pressure of the fluid through the kinetic energy of rotation; radial diffuser, responsible for transforming the dynamic pressure obtained in the impeller into static pressure and, consequently, decreasing the flow velocity; and volute, responsible for directing the flow at the exit.

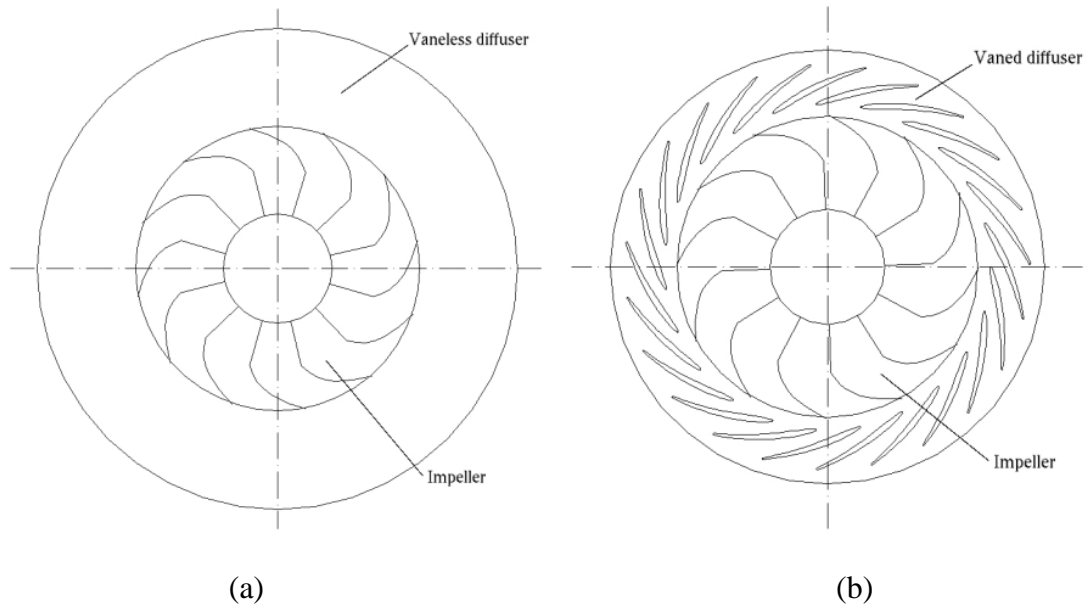
Fig. 1 Schematic of a centrifugal compressor.



Font: (HEINRICH, 2016).

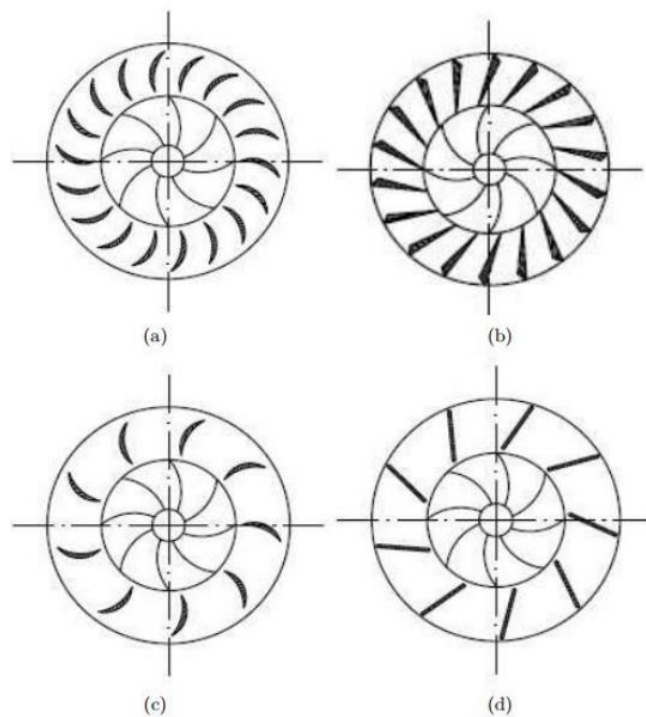
Within the category of diffusers, the geometry can be vaneless or vaned, as shown in Fig. 2. They differ in the construction of the channel since the second one has separated blades and the first one does not. The vaneless constructions, consequently, have lower efficiency due to rotor-stator interaction effects. However, vaned geometries have a smaller surge margin, as they are more susceptible to stall (TURUNEN-SAARESTI, 2004).

Fig. 2 Typical diffusers: (a) vaneless diffuser, (b) vaned diffuser.



Font: (Turunen-Saaresti, 2004).

Fig. 3 Typical vaned diffuser geometries: (a) cascade, (b) channel, (c) low-solidity, (d) low-solidity with plate vanes.

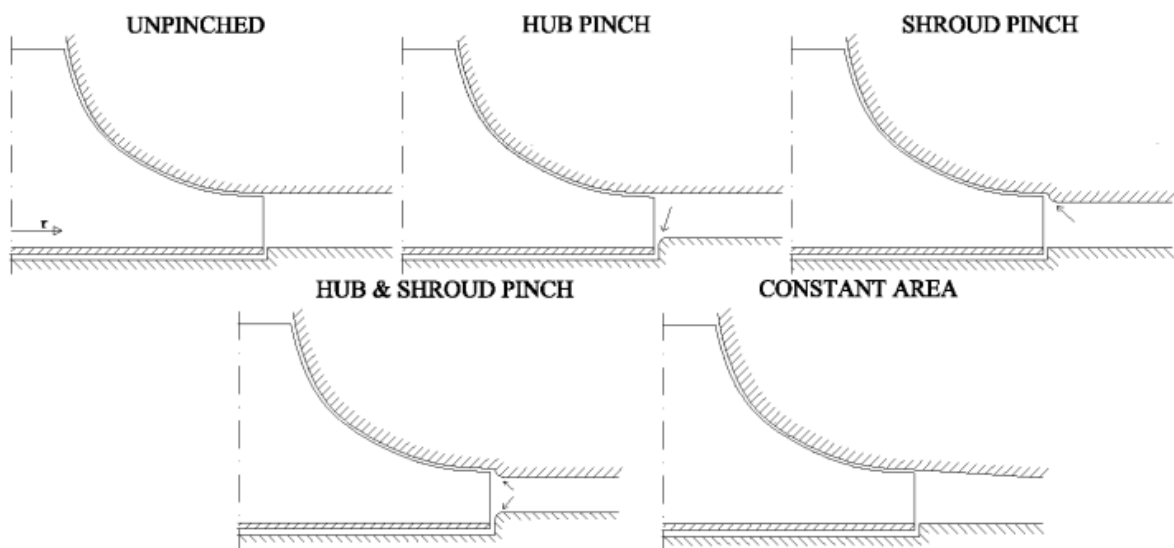


Font: (JAATINEN, 2009).

Within the vaned category, there are different types of vanes as can be seen in Fig. 3. Cascade and channel geometries have the best efficiencies and the smallest operating ranges and there is no evidence that one is superior to the other. The use will depend on the experience of the designer, and the need of the project (TURUNEN-SAARESTI, 2004). On the other hand, the low-solidity vaned diffusers feature a mix of vaned and vaneless geometry, increasing the operating range of vaned diffusers without penalizing the efficiency like those without vanes (TURUNEN-SAARESTI, 2004).

While within vaneless diffusers, the most common variations are pinches and area as shown in Fig. 4. The geometries with parallel walls have better efficiency and pressure recovery while the constant area one has a greater operating range, but lower efficiencies and the pinches are used to stabilize the flow at the impeller outlet (TURUNEN-SAARESTI, 2004).

Fig. 4 Different types of vaneless diffusers.



Font: (TURUNEN-SAARESTI, 2004).

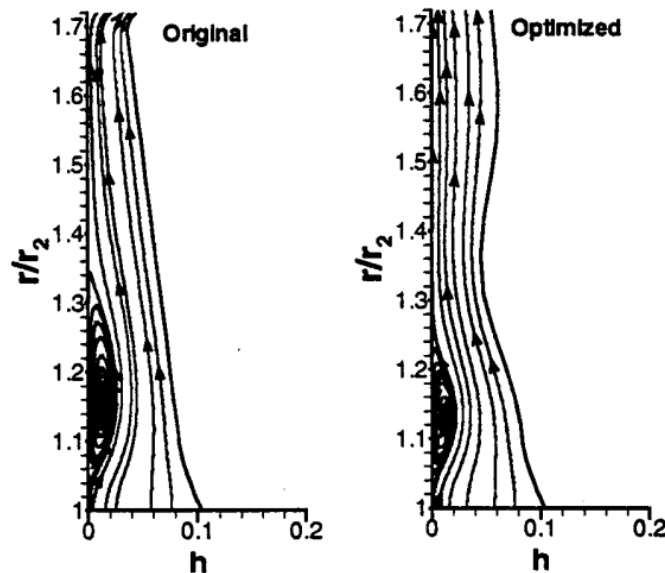
The diffuser plays an important role in compressor performance, since its geometry is directly linked to flow separation effects, transient rotor-stator interaction through the jet-wake pattern and other instabilities (DEAN; SENOO, 1960; ECKARDT, 1975; KRAIN, 1981; PINARBASI; JOHNSON, 1995) and, therefore, a proper sizing must be carried out. Nonetheless, most of the authors only rely on Aungier's book (AUNGIER, 2000b) loss models and experimental data (BRENES, 2014; WRIGHT et al., 2010). Recently, more modern

methods, such as three-dimensional simulation, have been approached due to the increase in computational capacity.

Turunen-Saaresti (2004), for example, performed a computational and experimental analysis of flow fields in diffusers. This study compared the performance variation of 11 types of diffuser construction and obtained an increment of 3% in total-to-total isentropic efficiency in addition to characterizing some phenomena of pinch geometries and transient flows as well as their effects on machine performance. However, the work did not use any optimization methodology, focusing only on the comparison between different known geometries and characterizing the respective fluid dynamic phenomena.

Shaaban (2015), on the other hand, used a genetic optimization algorithm applied to a RANS 2D axisymmetric modeling to vary the diffusion rate through divergent and converging channels to maximize the static pressure recovery coefficient by about 3.8% through the reduction of the total pressure loss coefficient by about 10%. Nevertheless, the optimal geometry submitted to a 3D simulation showed different results when compared to 2D.

Fig. 5 Original and optimized geometry of a vaneless diffuser channel.



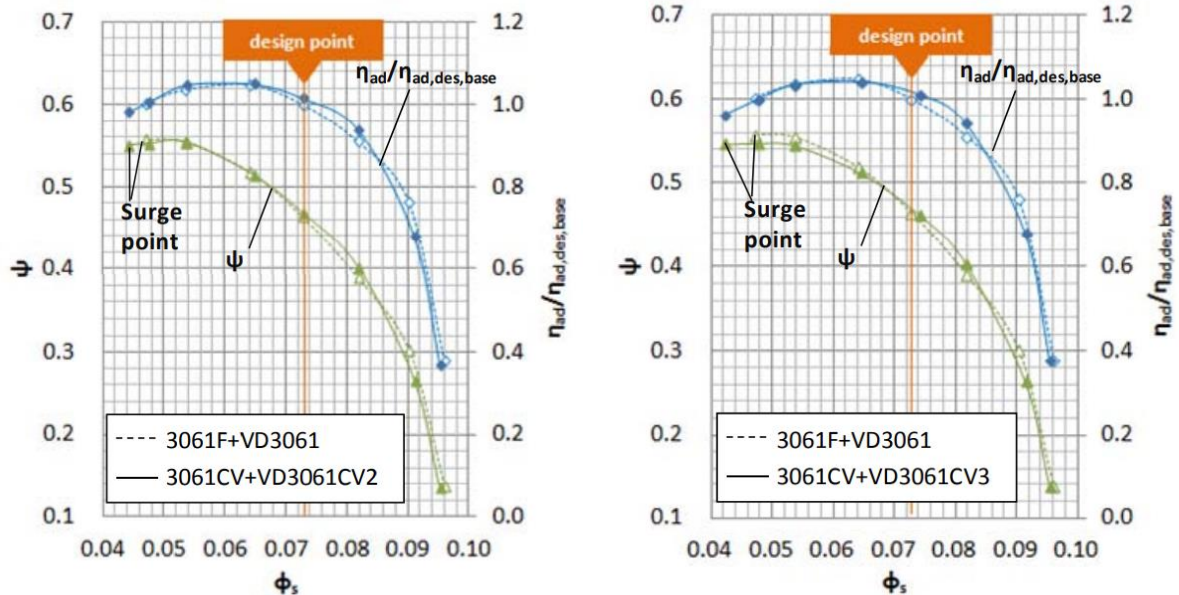
Font: (LEE; LUO; BEIN, 2000).

Lee et al. (2000) achieved 2.0% to 3.0% increase in isentropic efficiency by reducing a

recirculation close to the hub as can be seen in Fig. 5 through a direct optimization of the meridional shape on a vaneless diffuser. Despite the improvement found, the work evaluated only the change in the shroud and started from an initial geometry with parameters already known.

In addition to optimization/CFD coupling, surrogate and sensitivity analysis methods have been frequently used in complex models as centrifugal compressors to minimize computational effort. These tools allow identifying mathematical relationships between input and output variables such as the performance variation or intensity of a phenomenon as a function of geometry modifications, which reduces the simulation processing time required because it is possible to eliminate inputs that do not significantly affect the outputs and all subsequent processes can be analyzed through a mathematical metamodel (FORRESTER; SÓBESTER; KEANE, 2008).

Fig. 6 Pressure ratio (Ψ) and adiabatic efficiency (η) comparison between optimized (continuous line) and base geometries (dashed lines) in relation to flow coefficient (ϕ).



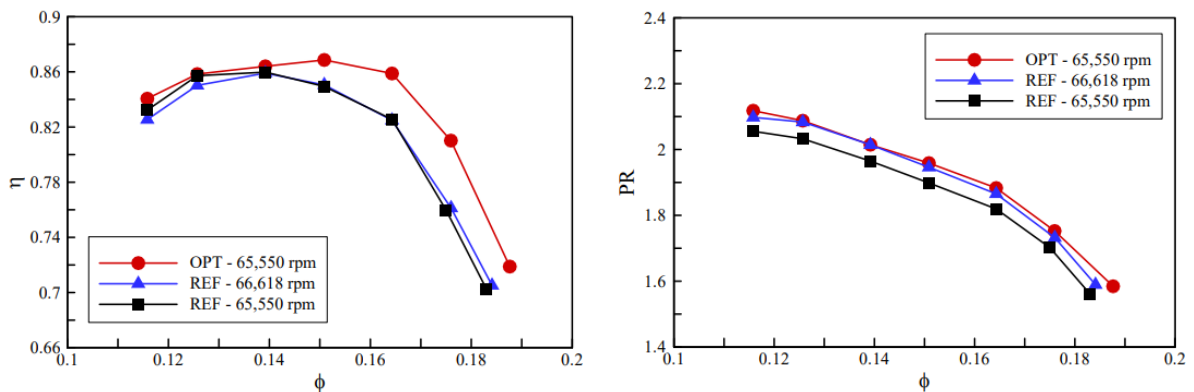
Font: (SUGIMURA; KOBAYASHI; NISHIDA, 2012).

Sugimura et al. (2012) used a multi-objective genetic algorithm coupled with the Kriging surrogate model and 3D RANS simulation to improve by 1.2-1.4% the adiabatic

efficiency at the design point and expand by 3.7-6.7% the surge margins of a centrifugal compressor by varying the shape of curvilinear element blades as shown in Fig. 6. Despite this, the process was conducted using a low-solidity vaned diffuser and only the angles were modified, therefore, the major enhancement was in the surge margin.

Kim et al. (2010) used a radial basis neural network surrogate technique with Uniform Latin Hypercube sampling method coupled to a multi-objective genetic algorithm to increase the isentropic efficiency by 0.65% and the pressure ratio by 1.4%, as shown in Fig. 7, through the variation of only the meridional shape of an impeller with 4 Bézier points.

Fig. 7 Comparison between performance parameters.

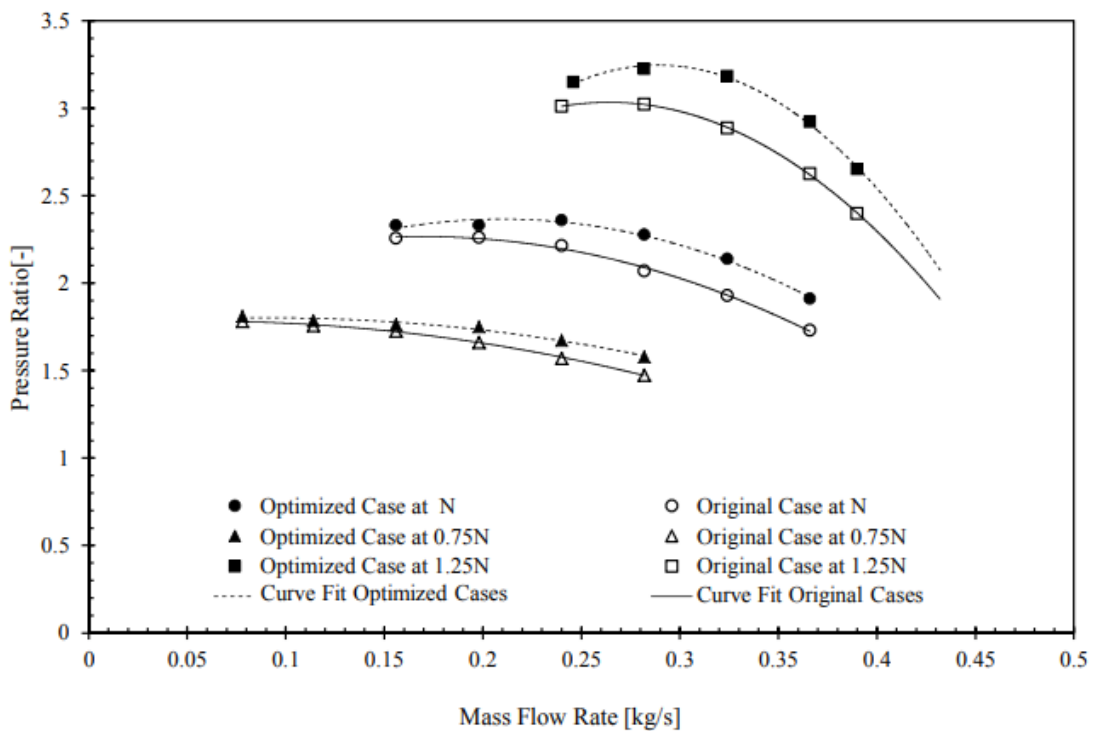
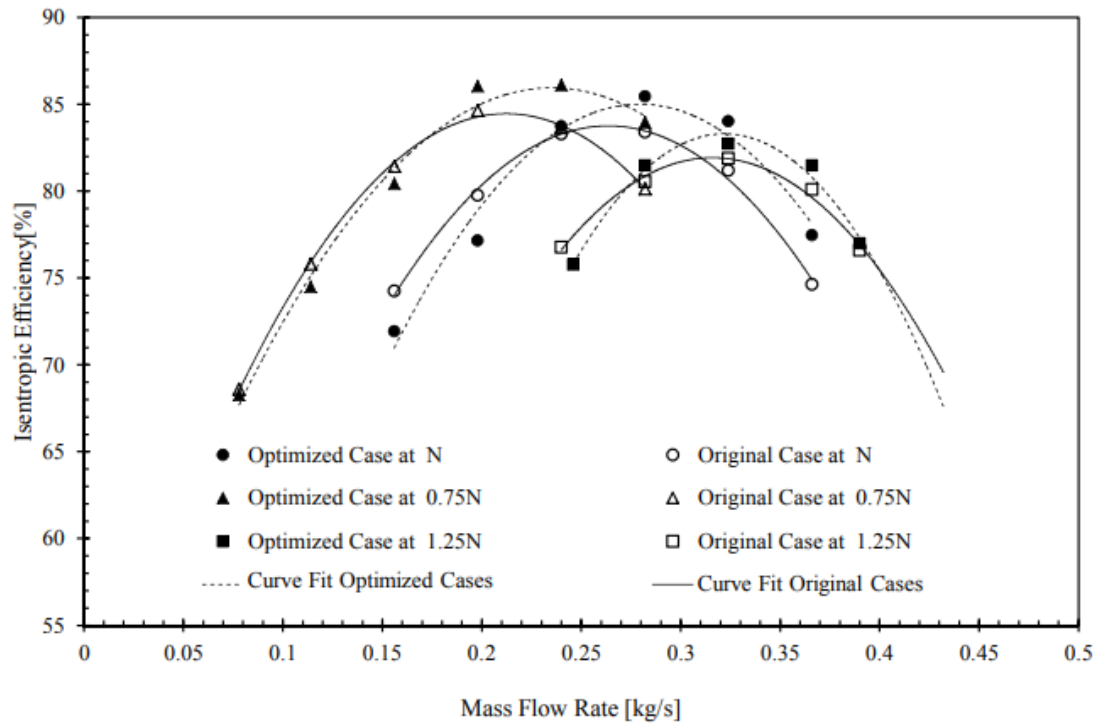


Font: (KIM et al., 2010)

He & Zheng (2017) used a metamodel based on an Artificial Neural Network (ANN) with 2 hidden layers to optimize the isentropic efficiency by 2.2% and increase the choke margin by 8.1% just by varying the camber, the sweep and the lean angles separately. They also performed a sensitivity analysis to identify the influence of each parameter on performance and a post-processing study to understand what such modifications represented in fluid dynamic phenomena.

However, the two studies mentioned above did not take into account diffuser parameters and did not use any method to eliminate variables. This limits some possibilities since the optimization time grows nonlinearly with the increase of variables.

Fig. 8 Performance analysis.

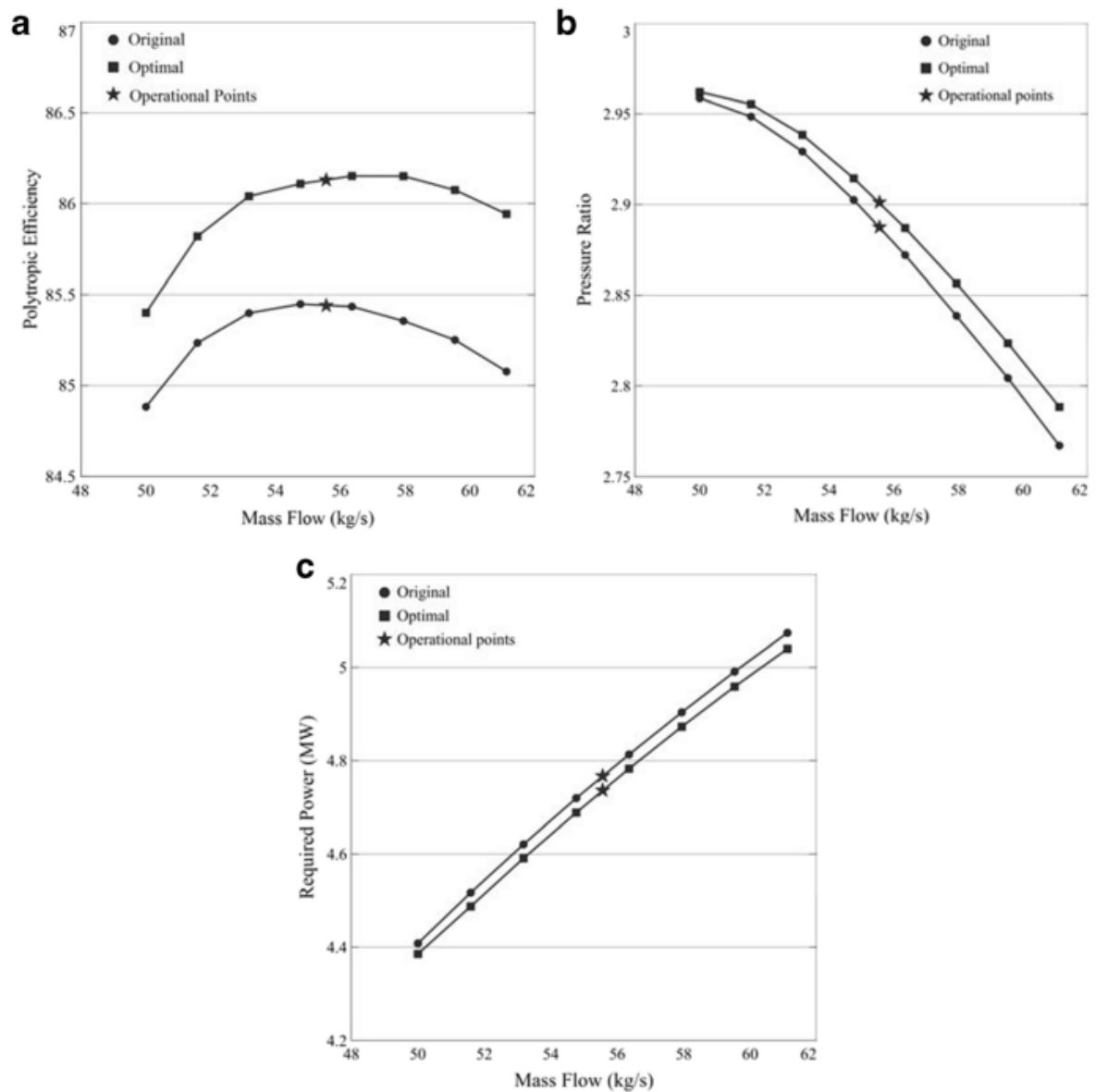


Font: (MOJADDAM; PULLEN, 2019).

Mojaddam & Pullen (2019), therefore, optimized the isentropic efficiency and the

pressure ratio by 3.0% and 11% respectively, as can be seen in Fig. 8, using the Box-Behnken method for 6 variables previously selected as the most influential in a total of 13 initials and consequently reducing the computational cost. The authors applied a Full Factorial method divided into three stages to identify the inputs that represented the most significant variations in the performance. The three stages were used to analyze separately the variation of the meridional geometry, the variation of the blade angles and the position of the leading edges. However, the authors performed separate analyses, neglecting interaction effects.

Fig. 9 Original and optimized performance parameters.



Font: (SALVIANO et al., 2021).

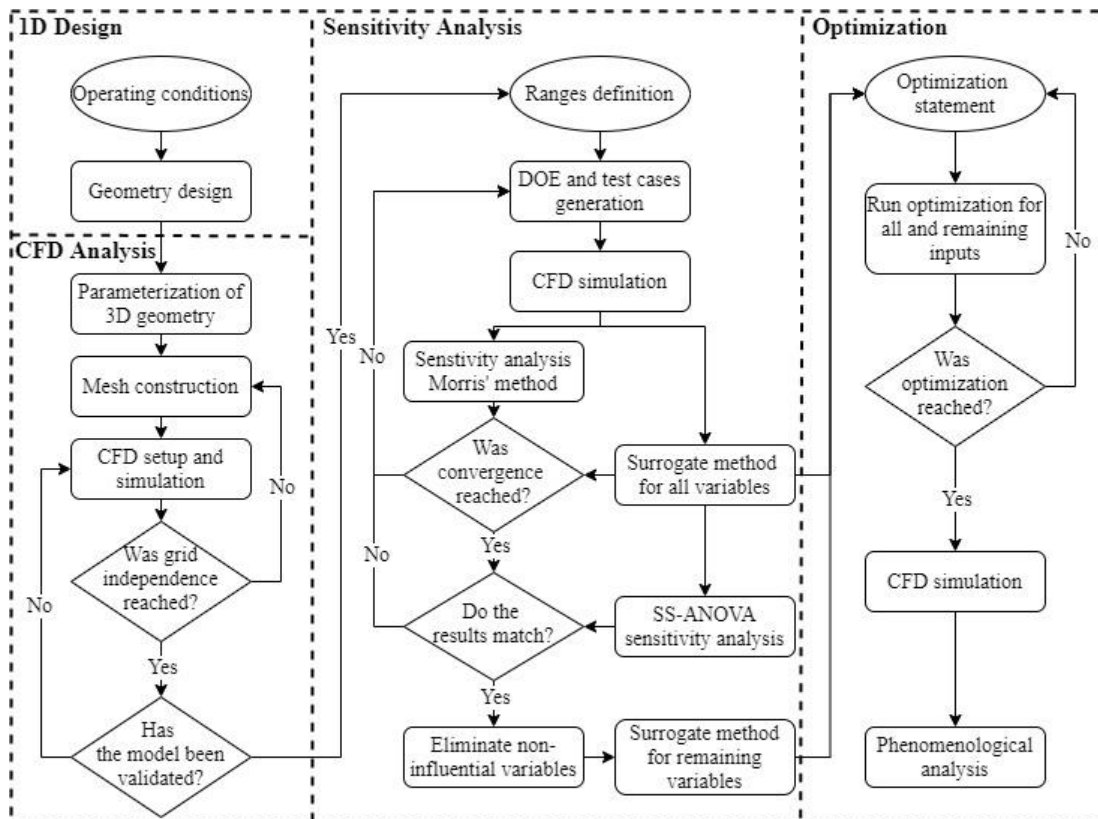
Salviano et al. (2021), on the other hand, optimized the polytropic efficiency of a carbon-dioxide centrifugal compressor by 0.7%, Fig. 9, varying eight blade angles using the Morris Elementary Effects as sensitivity analysis and a quasi-optimal sampling Design of Experiment (DoE) with 90 cases to train a surrogate model and to reduce the computational cost, reducing the number of geometric variables and representing the performance parameters as a mathematical function of the geometry.

However, except for this last work, the application of optimization to CO₂ compressors is quite new and when applied, they are not used to design geometry, but to improve something that already exists. And yet, few works take into account changes in the geometry of the diffusers, which have a high potential to improve performance.

3. METHODOLOGY

The vaneless-diffuser study conducted herein consisted in applying CFD-optimization and a sequential sensitivity analysis approach which are similar to the one proposed by Salviano et al. (2021) and by Mattos et al. (2019), as shown by the flowchart in Fig. 10. The impeller preliminary geometry was created using the software Ansys Vista CCD, a one-dimensional meanline prediction software (CASEY; ROBINSON, 2006), and imported into Ansys DesignModeler for parameterization of the input geometric variables. The mesh was generated using the software Ansys TurboGrid, an automatic software that produces a high-quality grid for turbomachinery components. The CFD modeling was submitted to a grid density study following the grid convergence index method (CELIK et al., 2008) and the results were validated by comparison with those results provided by meanline.

Fig. 10 Methodology flowchart.



Font: Prepared by the author.

Finally, three single-objective optimizations were conducted through the NSGA-II method (DEB et al., 2002) to increase total-to-total polytropic efficiency or static pressure recovery coefficient or to decrease total pressure loss coefficient. The optimization was performed using all variables and also using only those variables considered important by sensitivity analysis to confirm the reliability of the factor-fixing study. The results obtained were discussed based on thermodynamic and fluid dynamic phenomena to find the main sources of the differences between baseline and optimal geometries.

Moreover, the one-dimensional volute loss equations (AUNGIER, 2000c) were implemented in the validated model and the performance prediction of the entire compressor was submitted to the sequential sensitivity analysis that was conducted using a quasi-optimal sampling (GE; CIUFFO; MENENDEZ, 2015) for Morris elementary effects method (MORRIS, 1991) and also for response surface training. This surrogate was used to ensure the convergence of the number of routes (VANROLLEGHEM et al., 2015) and to run an analysis by the Smoothing Spline ANOVA method (GU, 2013) aiming to corroborate the Morris method.

3.1 GEOMETRY AND BOUNDARY CONDITIONS

The preliminary geometry of the impeller was built using a prediction meanline code (Ansys Vista CCD) proposed by Casey & Robinson (2006) which is a robust and user-friendly tool for high-performance centrifugal compressors design. For the present work, the geometric and aerodynamic inputs presented in Table 1 were used to build the three-dimensional geometry which was exported to Ansys BladeEditor to delimit the computational domain shown in Fig. 11. The vaneless-diffuser geometry was determined only by a channel of parallel plates without using one or two-dimensional design tools.

Due to the axisymmetric periodicity of the impeller and diffuser, the simulations needed only a passage with 1 main blade and 1 splitter and the results are extrapolated for the other 9 blades and splitters through a periodic interface boundary condition with a general grid interface (GGI) mesh connection method shown by *Symmetry* surfaces in Fig. 11. Moreover, the same method is applied to the impeller-diffuser interface, but in this case using multiple frames of reference (MFR) method called frozen-rotor (“ANSYS CFX-Solver

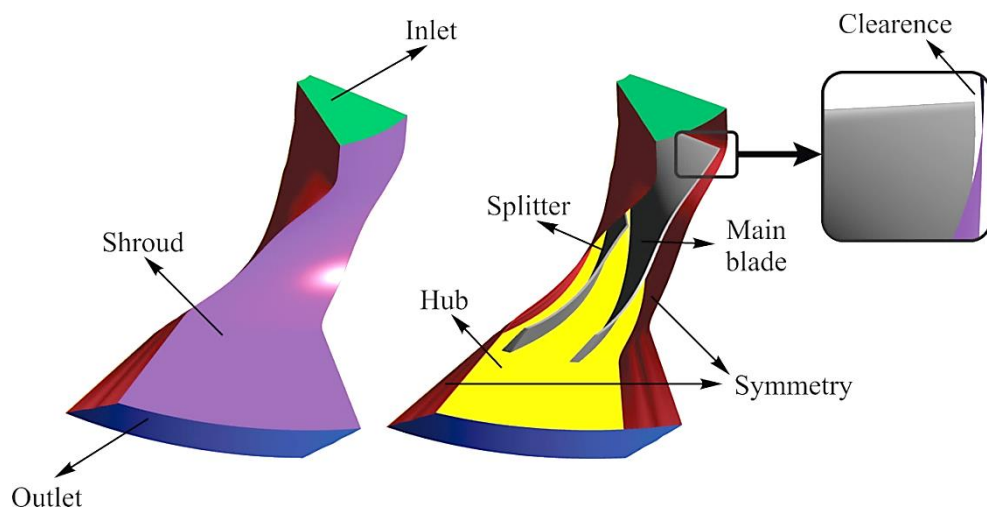
Theory Guide”, 2009), a suitable approach for flux conservation when there is a static surface in contact with a rotative surface.

Table 1 Geometrical parameters and boundary conditions.

Overall pressure ratio	2.85
Mass flow	55.56 kg/s
Rotational speed	12500 rpm
Inlet stagnation temperature	320 K
Inlet stagnation pressure	400 kPa
Hub diameter	70 mm
Hub thickness	10 mm
Shroud vane inlet angle	60°
Shroud thickness	3 mm
Diffuser	Vaneless
Axial tip clearance	1 mm
Number of blades and splitters	10 main blades and 10 splitters
Backsweep angle	45°
Rake angle	35°

Font: Prepared by the author.

Fig. 11 Computational domain with main components and boundary conditions indicated.



Font: Prepared by the author.

Hub and blades (main blade and splitter), indicated in Fig. 11, are set as no-slip and adiabatic rotating walls. The linear velocity vector \mathbf{U} can be represented mathematically by Eq. (1) for the stationary frame of reference and by Eq. (2) for the rotating frame of reference and the adiabatic flux q_w is represented by Eq. (3) where ω represents the angular velocity and \mathbf{R} represents the position vector.

$$\mathbf{U}_{wall,st} = \omega \cdot \mathbf{R} \quad (1)$$

$$\mathbf{U}_{wall,r} = 0 \quad (2)$$

$$q_w = 0 \quad (3)$$

Conversely, the shroud uses a no-slip and adiabatic counter-rotating wall method, where velocity is represented by Eq. (4) and Eq. (5) and adiabatic flux is represented by Eq. , because this surface remains stationary in centrifugal compressors with open and unshrouded impellers. Therefore, a clearance of 1 millimeter is created between these walls with different movements to prevent any interference.

$$\mathbf{U}_{st} = 0 \quad (4)$$

$$\mathbf{U}_r = -\omega \cdot \mathbf{R} \quad (5)$$

$$q_w = 0 \quad (6)$$

The inlet boundary conditions are prescribed stagnation pressure P_t and temperature T_t , Eq. (7) and Eq. (8) respectively, and fixed turbulence kinetic energy k and specific dissipation rate ω , calculated by Eq. (9) and Eq. (10) respectively. Where C_μ is a constant, L is the characteristic inlet scale and U_{ref} is the inlet flow velocity.

$$P_{t,st} = 400 \text{ kPa} \quad (7)$$

$$T_{t,st} = 320 \text{ K} \quad (8)$$

$$k = \frac{3}{2}(0.05U_{ref})^2 \quad (9)$$

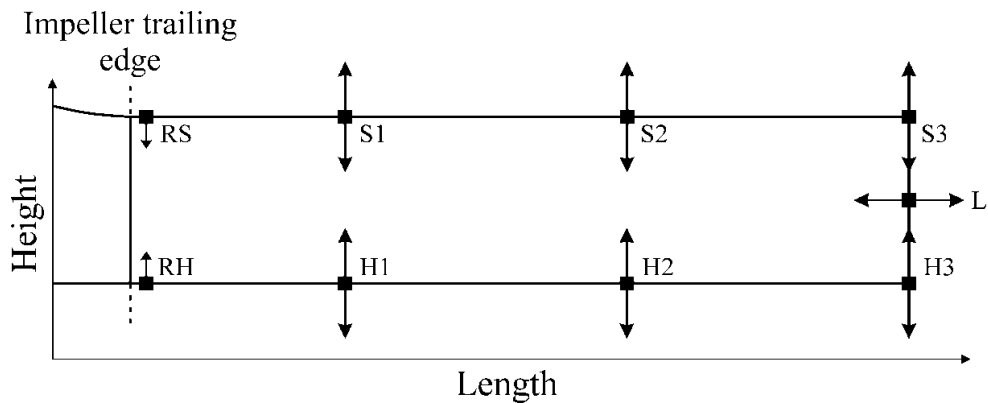
$$\omega = C_\mu^{\frac{3}{4}} \frac{k^{\frac{1}{2}}}{0.07L} \quad (10)$$

Finally, the output boundary condition was defined as uniform velocity in the stationary frame calculated by Eq. (11) from a known mass flow rate of 55.56 kg/s. Where ρ is the density and dA is the element surface area. This indirectly calculated velocity boundary condition is the standard compressor simulation model used by CFX due to the robustness of convergence.

$$U_{st} = \frac{\dot{m}}{\rho \int_S dA} = \frac{55.56}{\rho \int_S dA} \quad (11)$$

Control points evenly distributed have been defined along with the vaneless-diffuser domain as shown in Fig. 12, in which the shape of the geometry can be automatically modified during the simulations and optimization procedure. Variables RS and RH change the pitch at the diffuser inlet; H1, H2, H3, S1, S2 and S3 change the meridional shape and L changes the channel length. Those arrows represent, in scale, the freedom and the direction of movement of each variable.

Fig. 12 Geometrical parameters for optimization.



Font: Prepared by the author.

The variables of pinch (RS and RH) and channel length (L) were chosen due to the possible effects already mentioned such as flow stabilization, static pressure recovery and reduction and increase of recirculations. On the other hand, those that vary in meridional shape were inspired by Lee et al. (2000) due to the potential to deal with adverse pressure gradients.

Table 2 Variables range definition.

Input	Baseline [mm]	Lower [mm]	Upper [mm]
RH	0	0	2.50
H1	0	-4.00	4.00
H2	0	-4.00	4.00
H3	0	-4.00	4.00
L	200	190	210
RS	0	0	2.50
S1	39.6	35.6	43.6
S2	39.6	35.6	43.6
S3	39.6	35.6	43.6

Font: Prepared by the author.

A study of the numerical solution stability considering the upper and lower bound of the input variables is conducted to find critical points and these values, which are presented in Table 2. This approach ensures greater flexibility to turbomachinery design as it allows exploring designs that cannot be modeled by the meanline method due to experimental and analytical dependence.

3.2 DISCRETIZATION AND SOLUTION

Several studies on vaneless-diffuser concluded that the rotor-stator interaction has asymmetric and non-stationary characteristics. And, although the non-uniformities in the circumferential direction rapidly mix out along the channel, those in the axial direction persist until the outlet, especially in off-design operating conditions (DEAN; SENOO, 1960; ECKARDT, 1975; KRAIN, 1981; PINARBASI; JOHNSON, 1995).

However, even knowing that these transient and asymmetric effects impact compressor performance, the model was established using the steady-state transport equations for rotating domains implemented in Ansys CFX since the computational time for transient optimization is unfeasible for an optimization procedure.

This method works by solving flow in a rotating frame of reference that follows the rotational velocity of the compressor. This approach represents the impeller as a static domain, being able to calculate the relative velocity \mathbf{v}_r between the flow and the blades. Thus, it is necessary to include centrifugal and Coriolis forces to correct the flow as can be seen in momentum balance, Eq. (13). Also, the absolute velocity is inserted in the advection term to stabilize the solution when the relative velocity has high swirl behavior. Continuity, Eq. (12), and energy conservation, Eq. (14), are calculated in the same relative frame, so the rothalpy (I) substitutes the enthalpy to disregard the rotation effect (“ANSYS CFX-Solver Theory Guide”, 2009). At the end of each iteration, the solver uses the relative properties and fluxes to calculate the solution in the stationary frame for an inertial observer.

$$\nabla(\rho\mathbf{v}_r) = 0 \quad (12)$$

$$\nabla(\rho\mathbf{v}_r\mathbf{v}_{st}) = \nabla\bar{\tau}_r - \nabla P_r + \frac{S_{cr}}{2} + S_{cf} \quad (13)$$

$$\nabla(\rho\mathbf{v}_r I) = \nabla(k\nabla T_r + \bar{\tau}_r\mathbf{v}_r) \quad (14)$$

$$I = h + \frac{1}{2}[\mathbf{v}_r^2 - (\boldsymbol{\omega} \times \mathbf{r})^2] \quad (15)$$

In addition, the solver uses the two equation Baseline k- ω turbulence model modified by Menter (1994), called Shear-Stress Transport (SST), to account for the transport of turbulent shear stress, represented by Eq. (16) and Eq. (17), due to its good applicability for solutions with high adverse pressure gradients and flow separations. For this, the method presents a different way to calculate turbulence viscosity μ_t shown in Eq. (18) (“ANSYS CFX-Solver Theory Guide”, 2009).

$$\frac{d}{dx_j}(\rho U_j k) = \frac{d}{dx_j} \left[\left(\mu + \frac{\mu_t}{\sigma_{k3}} \right) \frac{dk}{dx_j} \right] - \beta' \rho k \omega \quad (16)$$

$$\frac{d}{dx_j}(\rho U_j \omega) = \frac{d}{dx_j} \left[\left(\mu + \frac{\mu_t}{\sigma_{\omega 3}} \right) \frac{d\omega}{dx_j} \right] + (1 - F1) \frac{2\rho}{\sigma_{\omega 2} \omega} \frac{dk}{dx_j} \frac{d\omega}{dx_j} + \beta_3 \rho \omega^2 \quad (17)$$

$$\mu_t = \frac{\rho \alpha_1 k}{\max(\alpha_1 \omega, SF_2)} \quad (18)$$

Where U_j is the velocity in j coordinate, x_j is the position along coordinate j , S is an invariant measure of the strain rate, $F2$ is a blending factor represented by Eq. (19) and β' , $\sigma_{\omega 2}$ and α_1 are constants. Also, all the constants with subindex 3 (σ_{k3} , $\sigma_{\omega 3}$, β_3) are calculated according to Eq. (20) using a blending factor $F1$ calculated by Eq. (21) since subindex 1 and 2 represent the constants from k- ϵ and standard k- ω respectively and y is the distance to the nearest wall.

$$F2 = \tanh \left\{ \left[\max \left(\frac{2\sqrt{k}}{\beta' \omega y}, \frac{500\mu}{\rho \omega y^2} \right) \right]^2 \right\} \quad (19)$$

$$\phi_3 = F1\phi_1 + (1 - F1)\phi_2 \quad (20)$$

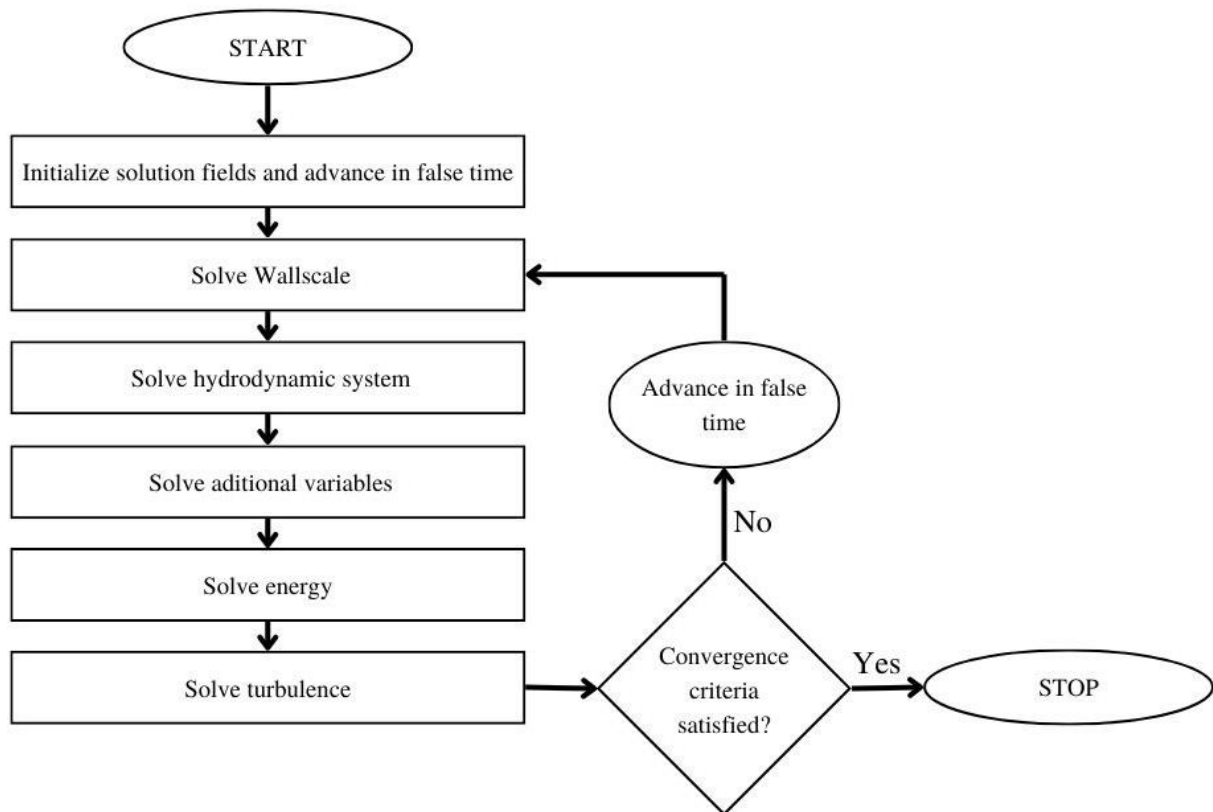
$$F1 = \tanh \left(\left\{ \min \left[\max \left(\frac{\sqrt{k}}{\beta' \omega y}, \frac{500\mu}{\rho \omega y^2} \right), \frac{4\rho k}{CD_{k\omega} \sigma_{\omega 2} y^2} \right] \right\}^4 \right) \quad (21)$$

$$CD_{k\omega} = \max \left(2\rho \frac{1}{\sigma_{\omega 2} \omega} \frac{\partial k}{\partial x_j} \frac{\partial \omega}{\partial x_j}, 10^{-10} \right) \quad (22)$$

An automatic near-wall treatment is also applied to supply the solution where the element does not reach the necessary refinement condition (“ANSYS CFX-Solver Theory Guide”, 2009).

The other thermodynamic variables is calculated using EOS proposed by Aungier Redlich-Kwong due to its good accuracy for dioxide carbon and its good agreement with supercritical states (AUNGIER, 1995).

Fig. 13 Solution method of ANSYS CFX for steady-state problems.



Font: Prepared by the author.

The coupled-solution method follows the organizational chart presented by the Fig. 13. Where the distance equations from the wall are first calculated to apply to the blending factor equations of the turbulence model. Then the momentum and continuity equations are solved using a momentum-like equation to each integration point, a strategy similar to that proposed by Rhie-Chow pressure-velocity coupling method (RHIE; CHOW, 1983) and modified by Majumdar et al. (1992) to remove the dependence on the time step. With the velocity and pressure field, it is possible to calculate the energy equation, obtaining the temperature, and then the turbulence equations, obtaining the turbulence kinetic energy and dissipation terms (“ANSYS CFX-Solver Theory Guide”, 2009).

These equations are applied to the discretized finite-volumes and a lot of suitable methods of discretization are used. First, the integral equations involving gradient and divergent operators are submitted to Gauss' Divergence Theorem to convert in surface integrals. Shape functions are applied to terms to account for the effects of the shape and

direction of element faces. Gradients at nodes are evaluated again using Gauss' Divergence Theorem. The advection scheme chosen, called High Resolution, uses a nonlinear recipe to determine a blending factor at each node based on the boundedness principle (BARTH; JESPERSEN, 1989) where zero means first order upwind and one means second order scheme. The diffusive terms and pressure gradient term are spatially discretized using the shape function approach adopted in finite elements. Finally, the discretization of the mass occurs through the pressure-velocity coupling equation already mentioned above and corrected by the linearized terms of compressibility (“ANSYS CFX-Solver Theory Guide”, 2009).

3.3 VOLUTE PERFORMANCE

Volute passages are complex three-dimensional components and would lead to a significant increase in processing cost if added to the RANS model. Instead, only a one-dimensional loss-based model was implemented to account for the effect of the volute on the compressor. The three loss equations are represented in Eq. (23), loss of the meridional velocity head, Eq. (24), tangential velocity head loss and Eq. (26), wall skin friction loss. Where the subindex i indicates volute inlet, o indicates volute outlet, m indicates meridional direction and U indicates tangential direction. Also, C indicates absolute velocity, r indicates radius, c_f indicates the friction coefficient and A indicates area.

$$\overline{w_m} = \left(\frac{C_{mi}}{C_i} \right)^2 \quad (23)$$

$$\overline{w_U} = \begin{cases} \frac{1}{2} \frac{r_i C_{Ui}^2}{r_o C_i^2} \left(1 - \frac{1}{SP^2} \right), & SP \geq 1 \\ \frac{r_i C_{Ui}^2}{r_o C_i^2} \left(1 - \frac{1}{SP} \right)^2, & SP < 1 \end{cases} \quad (24)$$

$$SP = \frac{r_i C_{Ui}}{r_o C_o} \quad (25)$$

$$\overline{w_{sf}} = c_f \left(\frac{C_o}{C_i} \right)^2 \frac{\pi^{\frac{3}{2}} (r_i + r_o)}{\sqrt{A_o}} \quad (26)$$

These loss terms were implemented in the post-processing stage to account for the effect of the volute in the analysis and were discounted from the total pressure at the diffuser outlet.

3.4 GRID ANALYSIS AND NUMERICAL VALIDATION

The discretization of the main domain is built using Ansys TurboGrid software due to the ease and high quality of the elements. To ensure the independence of the results concerning the number of elements, the Grid Convergence Index (GCI) method (CELIK et al., 2008) is applied. The low values of GCI and the negligible variations between the medium and fine grid presented in Table 3 confirm this independence and, therefore, the intermediate mesh can be used for future analyses. The three meshes used for convergence criteria analysis can be seen in Fig. 14.

Table 3 Grid independence analysis and numerical validation.

Case	Cells	r	Polytropic efficiency	Isentropic efficiency	Pressure ratio	Power
Vista CCD	-	-	86.4%	82.4%	2.85	4709 kW
Coarse grid	1352896	-	87.5%	85.9%	3.04	4877 kW
Medium grid	2987108	1.31	85.3%	83.5%	2.93	4828 kW
Fine grid	6429760	1.29	85.2%	83.4%	2.92	4814 kW
GCI₃₂			0.15%	0.16%	0.48%	0.52%
Validation			1.27%	1.33%	2.81%	2.53%

Font: Prepared by the author.

Furthermore, due to the lack of experimental data for carbon-dioxide centrifugal compressors and to guarantee that the present modeling is robust and reliable, the results were compared and showed good agreement with those predicted by the meanline method (Vista CCD), as shown by the difference, less than 3% for all output parameters, in Table 3. The meanline code is consistent with more than 45 different compressors with an efficiency precision of $\pm 2\%$ (CASEY; ROBINSON, 2006), therefore, is a reliable way to perform validations. Thus, the present numerical method can reproduce the behavior of a CO₂

centrifugal compressor and is suitable for the present work.

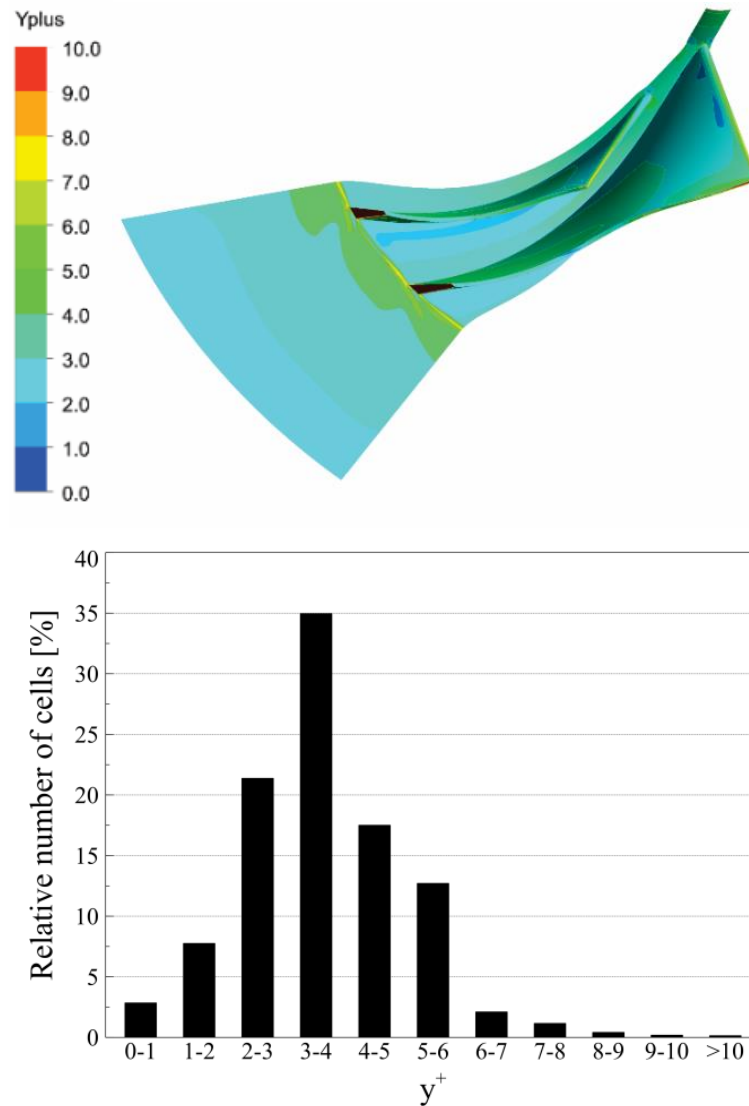
Fig. 14. Meshes used in the analysis: (a) coarse, (b) medium, (c) fine.



Font: Prepared by the author.

Fig. 15 shows the agreement of the mesh and the turbulence criteria with near-wall treatment since the maximum value of y^+ is less than ten and the average is between 3 and 4, which is considered satisfactory for flow analysis for high complexity models as centrifugal compressors (SALVIANO et al., 2021).

Fig. 15. Y-plus distribution in the domain to ensure turbulence quality criteria.



Font: Prepared by the author.

This parameter is very important to ensure that all boundary layer effects are captured and for this, low values are required, indicating that the mesh element closest to the wall is small enough to capture such effects. However, the more refined the mesh, the longer the pro-

cessing time and also the aspect ratio, which can lead to convergence problems. Therefore, to avoid these problems, a mesh with y^+ less than 10 represents a good agreement with the criteria (SALVIANO et al., 2021).

3.5 SENSITIVITY ANALYSIS

Sensitivity analysis is an interesting tool that has become popular in engineering and can be very useful in complex problems such as optimization in fluid dynamics as can be seen with different techniques (Salviano et al. (2021), Mattos et al. (2019), He & Zheng (2017) and Mojaddam & Pullen (2019)). Its goal is to evaluate the changes in output variables in relation to a change in input variables. A simple and effective qualitative method called Elementary Effects, presented in Eq. (27) and proposed by (MORRIS, 1991) is used to screen the space sample, provided by a quasi-optimal sampling method with 10 trajectories (CAMPOLONGO; CARIBONI; SALTELLI, 2007), to obtain a classification of the influence of each geometric variable in relation to the desired performance parameters. This approach results in a DoE with 100 runs ($r(k + 1)$). For this, two measures are evaluated, the mean Elementary Effect modified by Saltelli et al. (2007) (μ^*) and the standard deviation (S^2) of each input variable as can be seen in Eq. (28) and (29), respectively.

$$EE_i = \frac{Y(X_1, X_2, \dots, X_i + \Delta, \dots, X_k) - Y(X_1, X_2, \dots, X_i, \dots, X_k)}{\Delta} \quad (27)$$

$$\mu_i^* = \frac{1}{r} \sum_{j=1}^r |EE_i^j| \quad (28)$$

$$\mu_i^* = \frac{1}{r-1} \sum_{j=1}^r \left(EE_i^j - \frac{1}{r} \sum_{k=1}^r EE_i^k \right)^2 \quad (29)$$

where r is the number of trajectories defined by selecting the 10, in a sample space of 1000 configurations, with the largest spread, which is based on the distance between a couple of trajectories (m and l) presented in Eq. (30), where k is the number of input variables and

$X_i^m(z)$ indicates the z^{th} coordinate of the i^{th} input of the m^{th} trajectory.

$$d_{ml} = \begin{cases} \sum_{i=1}^{k+1} \sum_{j=1}^{k+1} \sqrt{\sum_{z=1}^{k+1} [X_i^m(z) - X_j^m(z)]}, & m \neq l \\ 0, & otherwise \end{cases} \quad (30)$$

Moreover, to corroborate this classification a quantitative sensitivity analysis method implemented in software ModeFRONTIER called Smoothing Spline ANOVA (GU, 2013) is also evaluated using a ULH (Uniform Latin Hypercube) sampling (MCKAY; BECKMAN; CONOVER, 1979) through the surrogate model. SS-ANOVA can identify the first-order interaction effects among the variables and classify them comparatively with the elementary effects to enrich the analysis.

3.6 SURROGATE MODEL

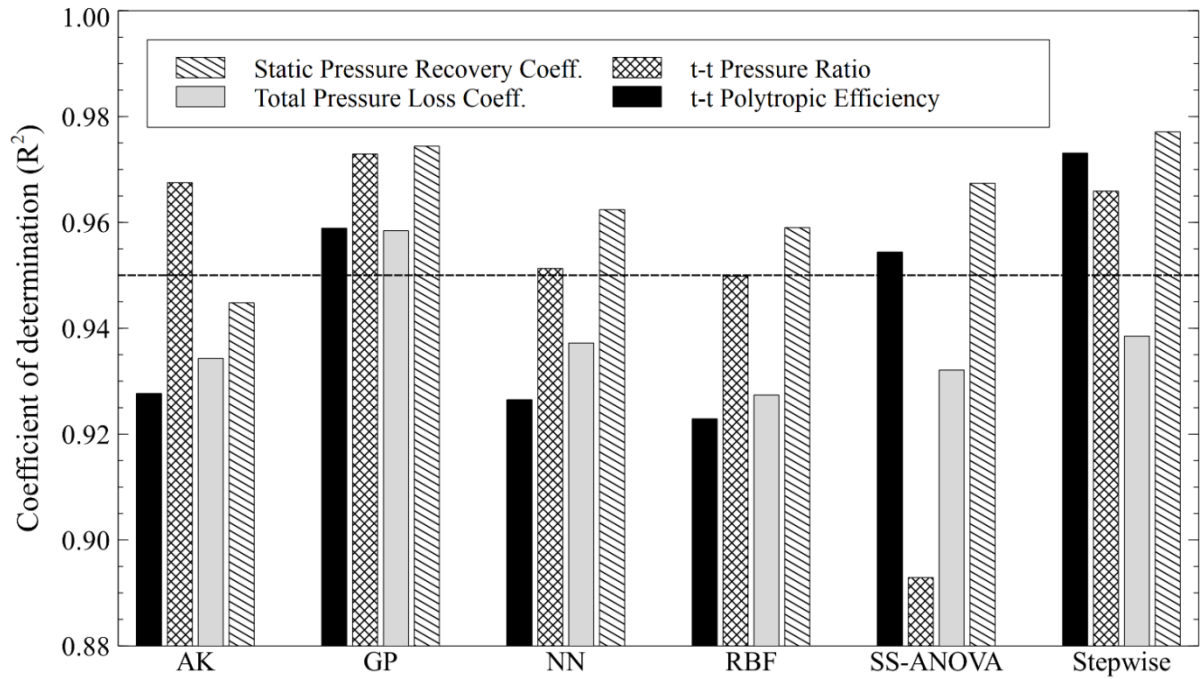
For high-dimensional problems such as centrifugal compressors whose performance depends on several geometric parameters, optimization through 3D RANS calculation may become unfeasible due to the high processing cost. Therefore, a suitable response surface method is an excellent tool because it replaces the complex model with a mathematical relationship between inputs and outputs.

Fig. 16 presents a comparison between the coefficient of determination of all response surfaces (RS) methods performed for four outputs. Gaussian Process (GP) regression was chosen for presenting the best overall coefficient of determination and the smallest maximum (less than 1.5%) and mean (less than 0.7%) errors. Therefore, this metamodel was used for Morris convergence study, Smoothing Spline ANOVA sensitivity analysis and optimization procedure.

All the RS training was conducted using the same quasi-optimal sampling from the Morris sensitivity analysis as suggested by Salviano et al. (2021) for nine variables and ten trajectories and the quality test was evaluated by other ten cases (10% of the sampling)

generated through Uniform Latin Hypercube Sampling (ULHS) (MCKAY; BECKMAN; CONOVER, 1979).

Fig. 16 Comparison between surrogate methods.



Font: Prepared by the author.

3.7 OPTIMIZATION

For the present work, three unconstrained optimization procedures through the response surface are performed separately. These approaches use the same geometry parameter vector shown in Eq. (31) and in concordance with Table 2.

$$X = \{RH, H1, H2, H3, L, RS, S1, S2, S3\} \quad (31)$$

The first objective function is defined by Eq. (32) which aims to maximize the total-to-total polytropic efficiency η_p of the entire centrifugal compressor (Optimization A) using

the thermodynamic model proposed by Mallen & Saville (1977), the other is related to minimize the total pressure loss coefficient ξ_p (AUNGIER, 2000d) of diffuser represented by Eq. (33) (Optimization B) and then to maximize static pressure recovery coefficient c_p (AUNGIER, 2000d) of the diffuser (Optimization C) as shown in Eq. (34).

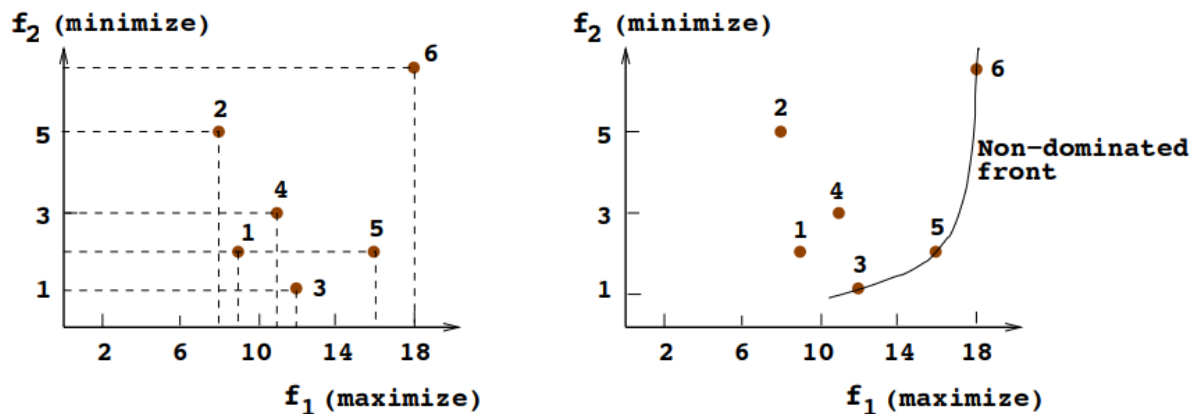
$$\text{Maximize } \eta_p(X) = 1 - \frac{(s_{vo} - s_{ii})(T_{tvo} - T_{tii})}{(h_{tvo} - h_{tii}) \ln\left(\frac{T_{tvo}}{T_{tii}}\right)} \quad (32)$$

$$\text{Minimize } \xi_p(X) = \frac{P_{tdi} - P_{tdo}}{P_{tdi} - P_{sdi}} \quad (33)$$

$$\text{Maximize } c_p(X) = \frac{P_{tdi} - P_{tdo}}{P_{tdi} - P_{sdi}} \quad (34)$$

The optimization was conducted using the NSGA-II method (DEB, 2011) with an initial population of 50 individuals generated by Uniform Latin Hypercube sampling and the convergence was found after about 100 generations.

Fig. 17 Non-dominated fronts.



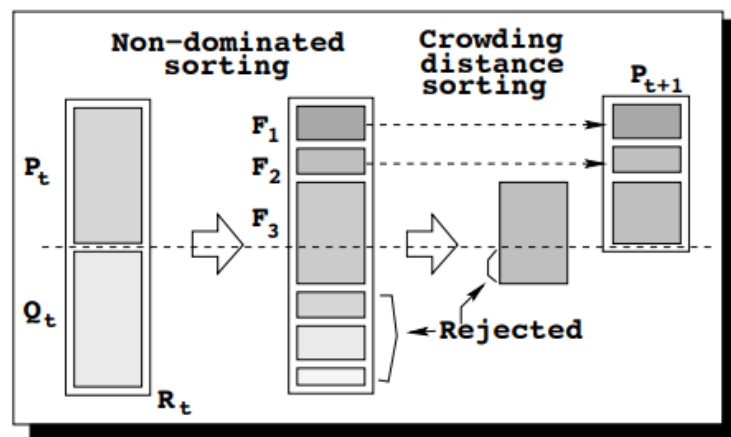
Font: (DEB, 2011).

This method works by searching non-dominated fronts in each new population as shown in Fig. 17 and rejecting the frontiers that are below the threshold as shown by the Non-

dominated sorting in Fig. 18. Then, a crowding distance sorting is realized by eliminating those points from the last frontier that fell below the threshold as can be seen in Fig. 18. After each sorting, a new population is generated through mutation and cross-over between the remaining individuals until convergence is reached (DEB, 2011).

As can be seen, this method is a multi-objective approach while the work presented here aims to optimize the geometry for three different single-objective functions. However, a method called multi-objectivization which modifies the function using a second objective based on maximizing the distance between individuals in the population. This allows the method to be applied to single-objective functions and it is able to prevent the program from converging to local maxima (SEGURA; SEGREDO; LEÓN, 2013).

Fig. 18 Sorting algorithm.



Font: (Deb, 2011).

4. RESULTS AND DISCUSSIONS

This section presents the sensitivity analysis and optimization results for the vaneless-diffuser to improve the performance of a sCO₂ centrifugal compressor with geometrical parameterization with nine geometric variables and for four important output variables.

For the first step, a sequential sensitivity analysis was performed to indicate and eliminate from the optimization process those geometric parameters which not significantly change the output variables. And, to confirm the robustness, the convergence test and another sensitivity analysis method through the response surface were performed. Finally, the optimization method was conducted with three different single-objective functions: maximize the total-to-total polytropic efficiency, minimize total pressure loss coefficient or maximize the static pressure recovery coefficient.

4.1 SEQUENTIAL SENSITIVITY ANALYSIS

The quasi-optimal sampling method was applied to 100 cases simulated via CFD and the mean elementary effects of Morris were calculated for each geometric variable of the vaneless-diffuser. The respective classification of the influence of each input variable in compressor performance parameters is presented in Fig. 19 for total-to-total polytropic efficiency, Fig. 21 for static pressure recovery coefficient, Fig. 20 for total-to-total pressure ratio and Fig. 22 for total pressure loss coefficient.

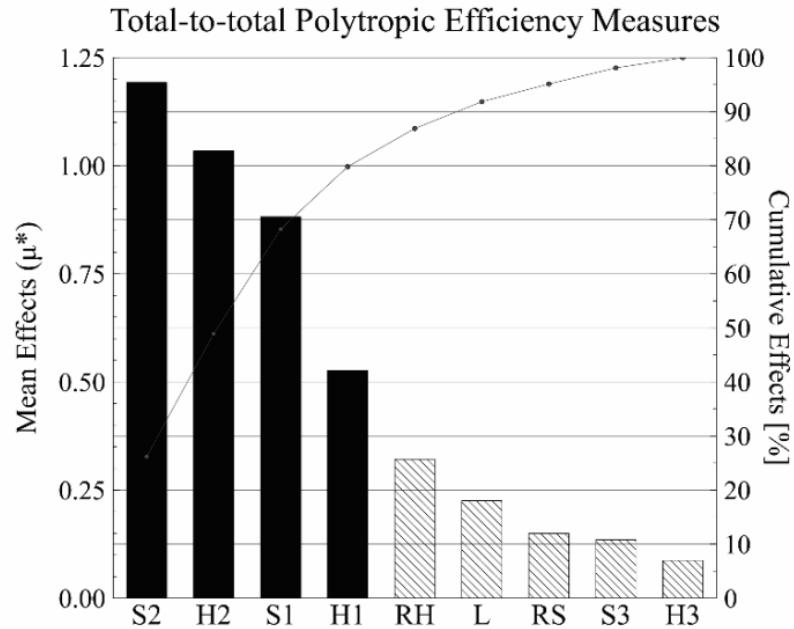
For polytropic efficiency, only the intermediate inputs (H1, S1, H2, S2) are important. Thus, this parameter does not change significantly with changes in the inlet and outlet of the channel. For pressure ratio, just the outlet parameters (H3, S3 and L) were non-influential.

And for static pressure recovery and total pressure loss, in addition to the outlet variables H3 and S3, the inlet input H1 also is non-influential. Furthermore, for the second performance parameter, the pinch at the shroud is a fourth negligible variable.

In summary, the inputs variables H3 and S3 were the only ones that are non-influential for all outputs evaluated, considering an approach for 80% of the accumulated effects. Therefore, such variables can be fixed at their original value without compromising future

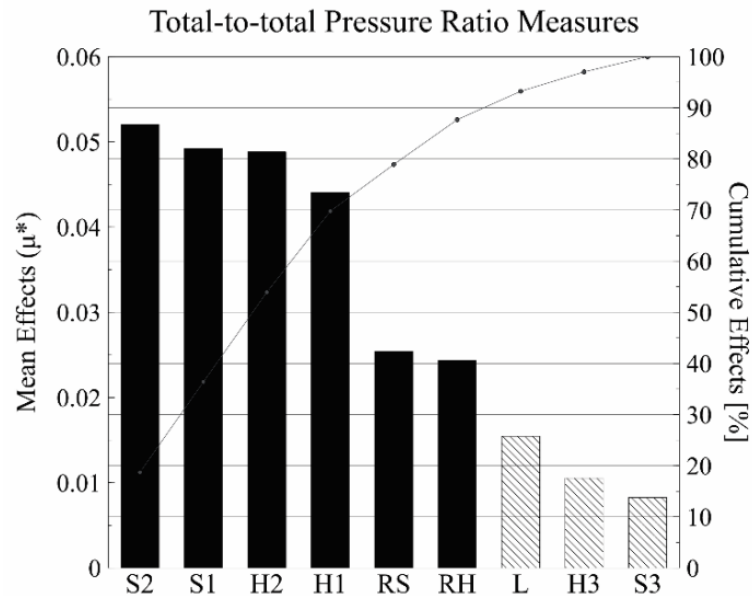
analyses and reducing the number of necessary simulations. Conversely, the intermediate variables H2, S2 appeared as highly influential for all outputs and the channel length L is only important for total pressure loss and static pressure recovery coefficients.

Fig. 19 Elementary effects for polytropic efficiency.



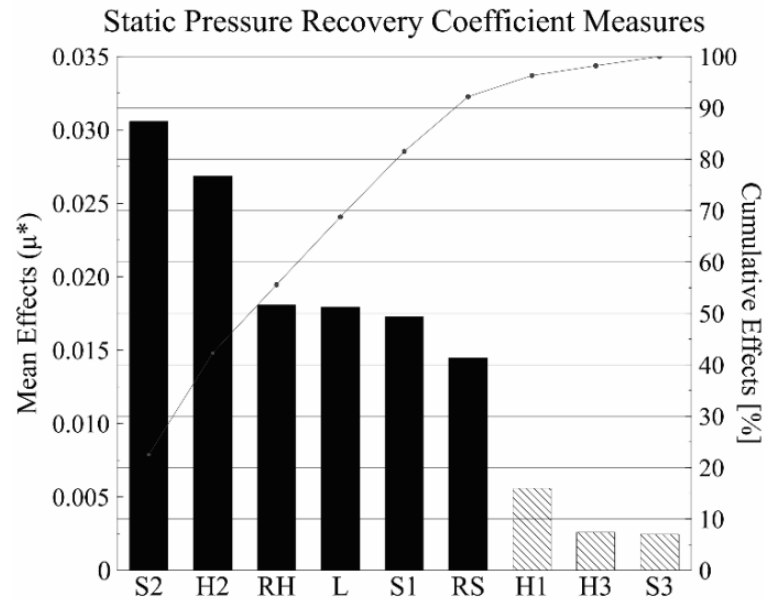
Font: Prepared by the author.

Fig. 20 Elementary effects for Polytopic Efficiency.



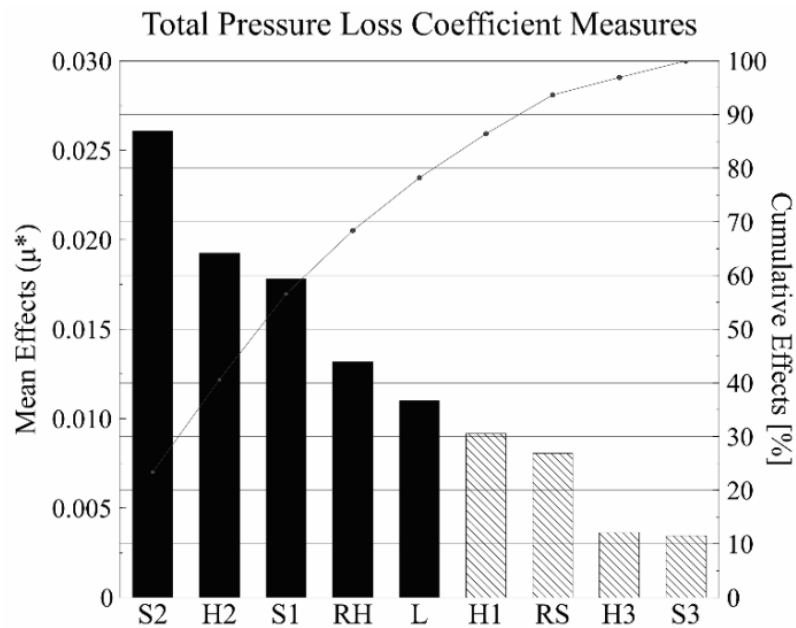
Font: Prepared by the author.

Fig. 21 Elementary effects for static pressure recovery.



Font: Prepared by the author.

Fig. 22 Elementary effects for Polytropic Efficiency.



Font: Prepared by the author.

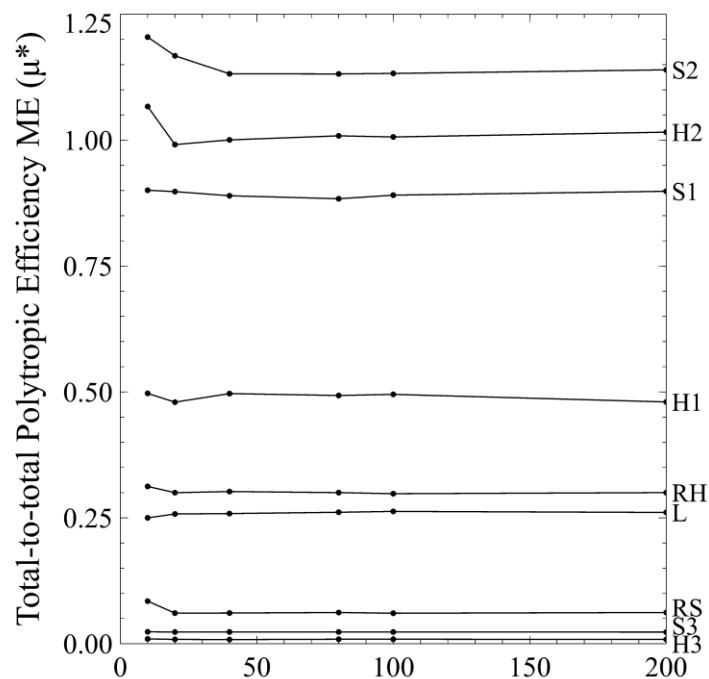
Phenomenologically, the impact of each input variable on dynamic flow is verified by sources of entropy generation and pressure loss, according to Denton (1993) and Bejan (2016), which explains the classification shown in Fig. 19, since the chosen performance

parameters are strongly related to these thermodynamic properties and it will be explained later in this chapter.

Moreover, a convergence study of the number of trajectories is conducted using a suitable metamodel (GP). The robustness of the method for factor-fixing purposes could be ensured even for 10 routes, as suggested by Saltelli et al. (2007), since the behavior of the variables presented in Fig. 23 for polytropic efficiency, Fig. 24 for static pressure recovery, Fig. 25 for pressure ratio and Fig. 26 for total pressure loss shows that, despite the slight variations, the ranking of inputs remained unchanged. Thus, the variables treated as non-influential would continue to represent the portion with the smallest impact even for high numbers of simulated routes.

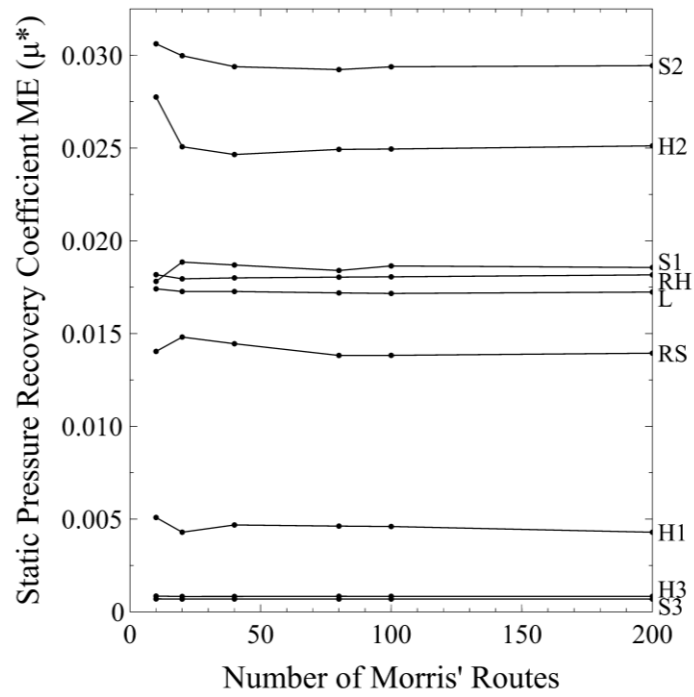
The geometric parameters of the shroud were better positioned in the ranking due to the proximity and ability to minimize the loss phenomena, similar to that found by Salviano et al. (2021) and Mattos et al. (2019) for impeller polar angles for t-t polytropic efficiency and t-t pressure ratio performance outputs.

Fig. 23 Convergence analysis of Morris method for polytropic efficiency.



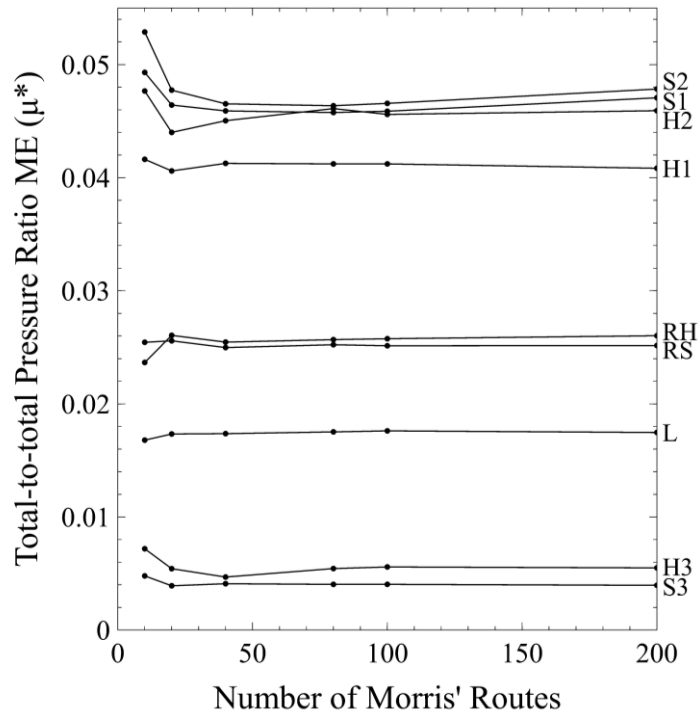
Font: Prepared by the author.

Fig. 24 Convergence analysis of Morris method for static pressure recovery.



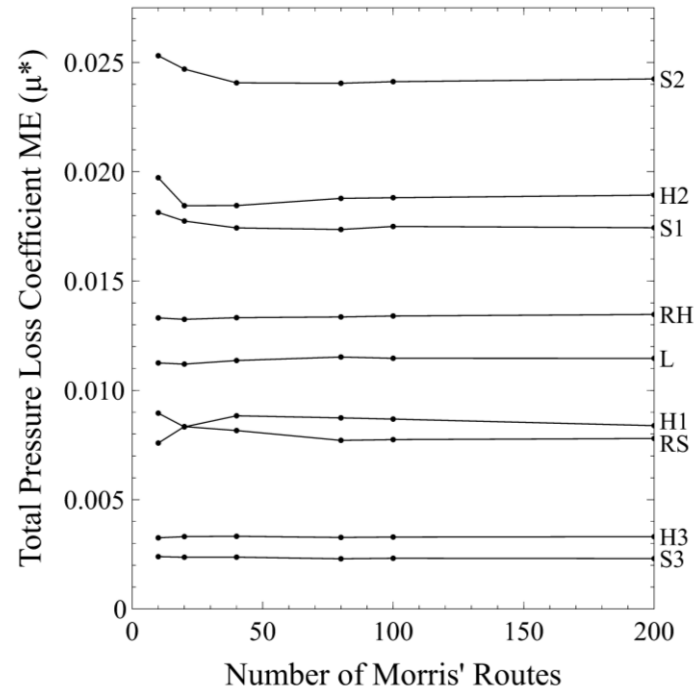
Font: Prepared by the author.

Fig. 25 Convergence analysis of Morris method for pressure ratio.



Font: Prepared by the author.

Fig. 26 Convergence analysis of Morris method for total pressure loss.



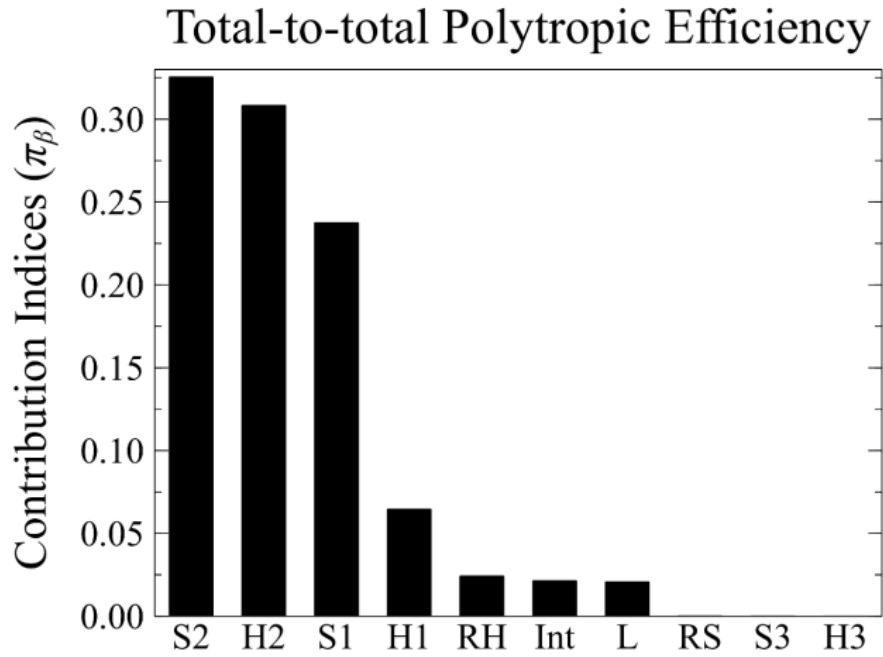
Font: Prepared by the author.

The major differences are located only in the variables with low influence. Therefore the method does not present the risk of classifying an influential variable as non-influential.

To corroborate these results, the SS-ANOVA sensitivity analysis was performed for a DoE with 729 cases generated by the ULHS sampling method and evaluated by the GP response surface. The highest collinearity indices ($\kappa\beta$) and the lowest coefficient of determination (R^2) found were 1.08 and 0.99, respectively, indicating that the study does not have identifiability problems and the regression fits well to the variables (GU, 2013).

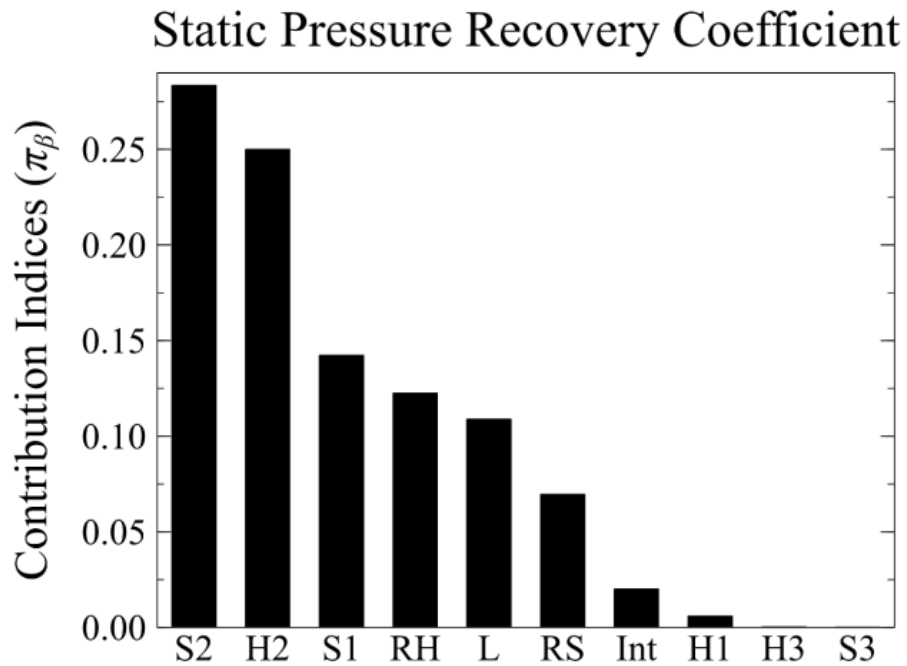
Fig. 27, Fig. 28, Fig. 29 and Fig. 30 indicate a similar ranking as that shown in Fig. 19, Fig. 20, Fig. 21 and Fig. 22, respectively, indicating the reliability of the elementary effects method for purposes of variable elimination for the subject under study. Furthermore, it reinforces that H3 and S3 have a negligible impact on the output variation of the compressor performance and also indicates the low influence of the interaction effects, shown by the abbreviation “Int” in the figure.

Fig. 27 Contribution indices from SS-ANOVA analysis for polytropic efficiency.



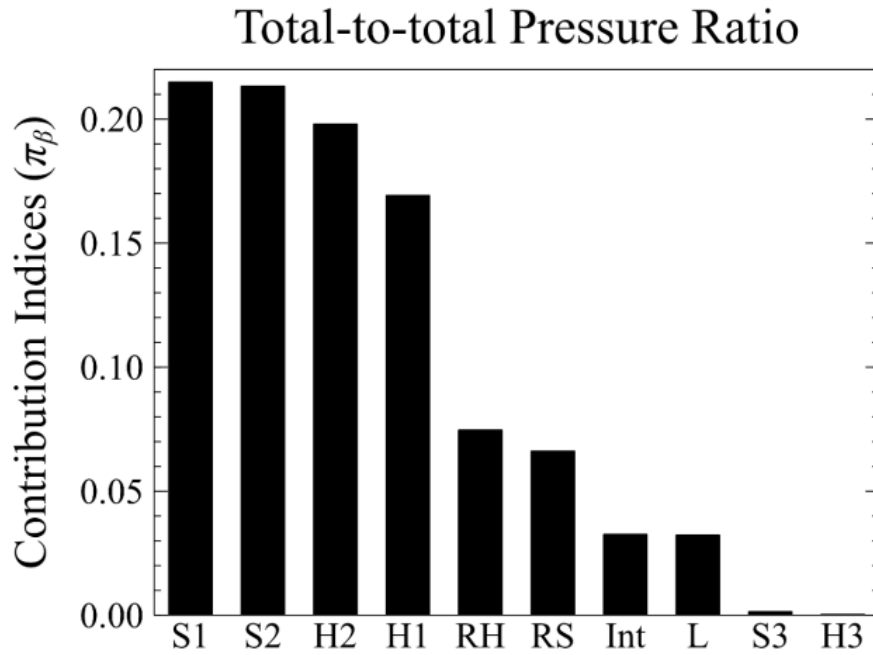
Font: Prepared by the author.

Fig. 28 Contribution indices from SS-ANOVA analysis for static pressure recovery.



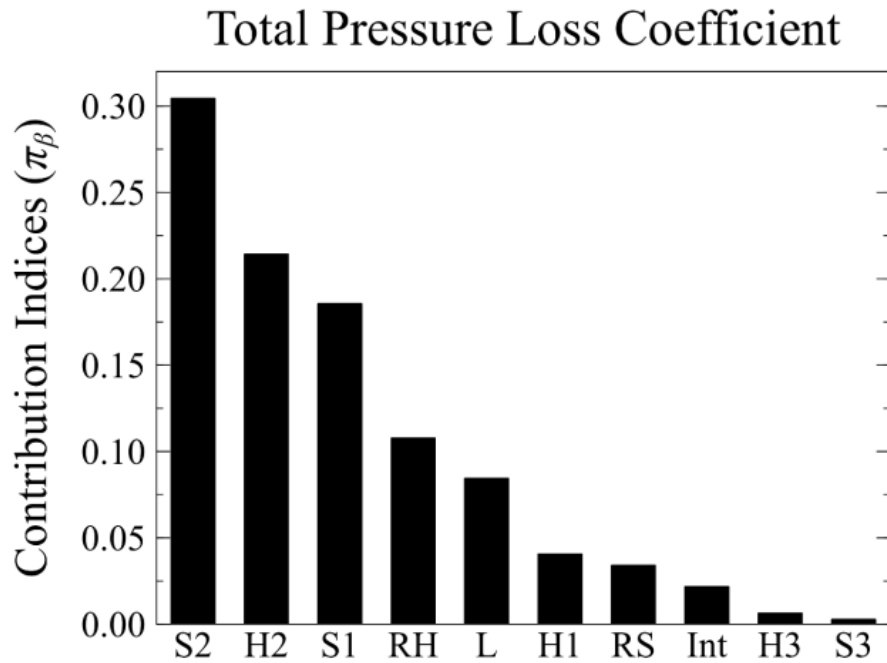
Font: Prepared by the author.

Fig. 29 Contribution indices from SS-ANOVA analysis for pressure ratio.



Font: Prepared by the author.

Fig. 30 Contribution indices from SS-ANOVA analysis for pressure loss.



Font: Prepared by the author.

4.2 OPTIMIZATION

An optimization process is conducted by two approaches: optimization of the output variables with all inputs and optimization of the output variables with remaining variables from the factor fixing study. Table 4 shows that Opt. A (optimal total-to-total polytropic efficiency) and Opt. B (optimal total pressure loss coefficient) presents the same geometry for 9 input variables and a similar geometry for 7 inputs since both objective functions tend to improve aerodynamic performance since the polytropic efficiency, different from isentropic efficiency, eliminates the thermodynamic effect of increasing the pressure ratio as stated by Aungier (2000b). Thus, optimizations A and B are treated as one since RS, the only parameter that changed does not represent a large variation in the results. Opt. C (optimal static pressure recovery coefficient) differs from other objective functions only for the length of the channel, since the extension increases static pressure recovery by reducing the meridional velocity and reduces the polytropic efficiency by increasing skin friction area as shown in Fig. 31.

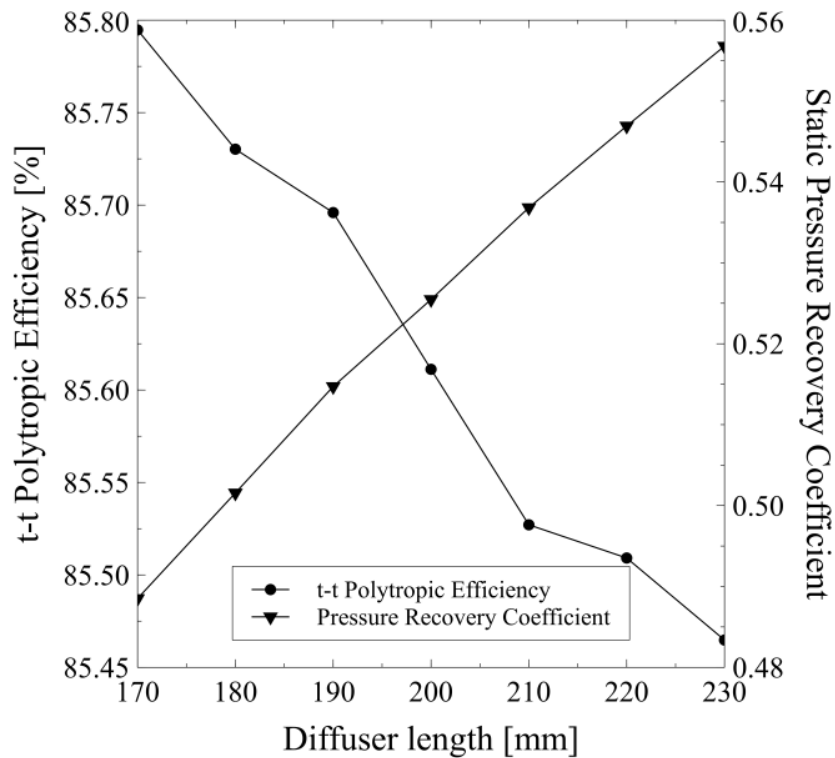
Table 4 Baseline and optimized geometries.

Variables [mm]	Baseline	Opt. A		Opt. B		Opt. C	
	-	9 inputs	7 inputs	9 inputs	7 inputs	9 inputs	7 inputs
RH.	0	0	0	0	0	0	0
H1	0	4.00	4.00	4.00	4.00	4.00	4.00
H2	0	4.00	4.00	4.00	4.00	4.00	4.00
H3	0	4.00	0*	4.00	0*	4.00	0*
L	200	190	190	190	190	210	210
RS	0	0	1.60	0	2.50	0	0
S1	39.6	35.6	35.6	35.6	35.6	35.6	35.6
S2	39.6	35.6	35.6	35.6	35.6	35.6	35.6
S3	39.6	35.6	39.6*	35.6	39.6*	35.6	39.6*

*Fixed values.

Font: Prepared by the author.

Fig. 31 Performance behavior along of the channel length.

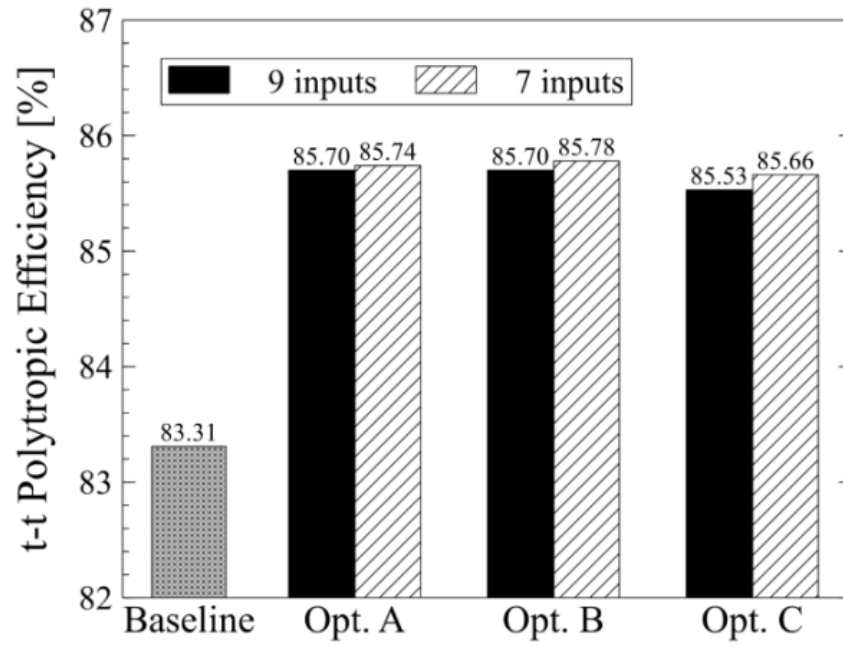


Font: Prepared by the author.

Table 4 also indicates that both approaches with 9 and 7 variables found similar optimal input parameters, except for those fixed by the sequential sensitivity analysis, which is also observed in the results presented in Fig. 32, Fig. 33 and Fig. 34, indicating the robustness of the factor-fixing method since the major relative differences are 0.15% for t-t polytropic efficiency, 0.66% for t-t pressure ratio, 0.56% for static pressure recovery coefficient and 3.1% for total pressure loss coefficient.

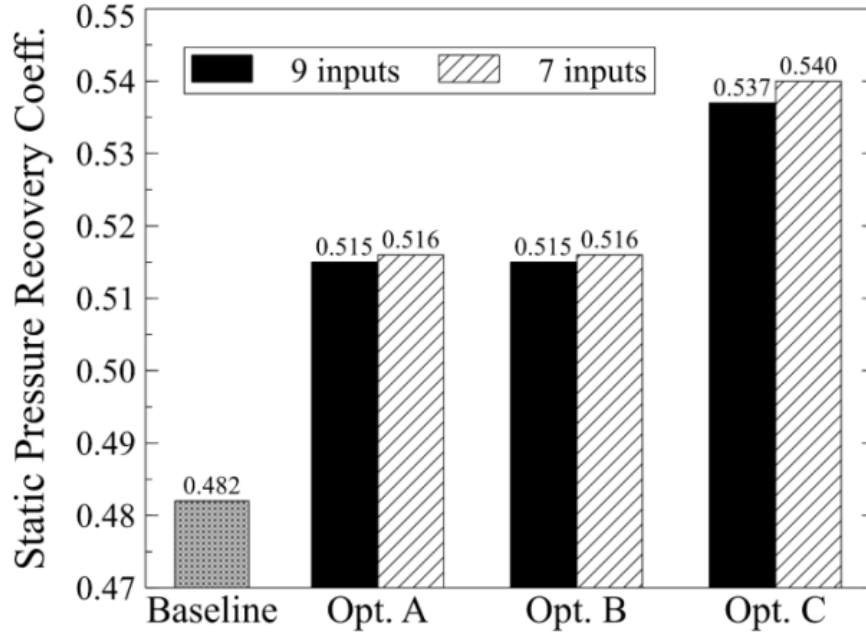
Moreover, the optimization results confirm the advantage of the methodology considering a coupling of sensitivity analysis method, CFD and optimization method to find the optimal centrifugal compressor, since the t-t polytropic efficiency had an increase of 2.87% shown in Fig. 32, the static pressure recovery coefficient had an increase of 11.4% shown in Fig. 33 and the total pressure loss coefficient had a decrease of 24.0% shown in Fig. 34.

Fig. 32 Optimal parameters for polytropic efficiency.



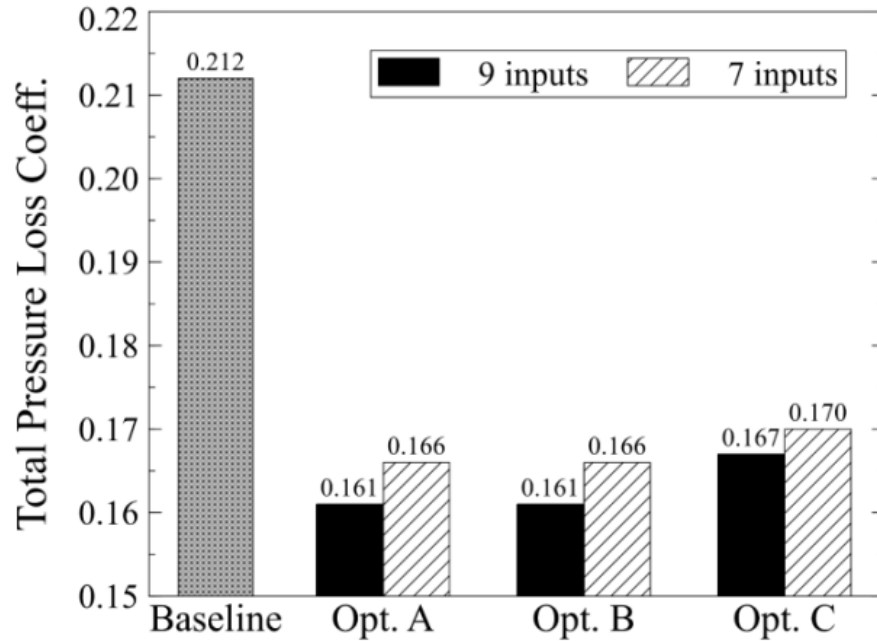
Font: Prepared by the author.

Fig. 33 Optimal parameters for static pressure recovery.



Font: Prepared by the author.

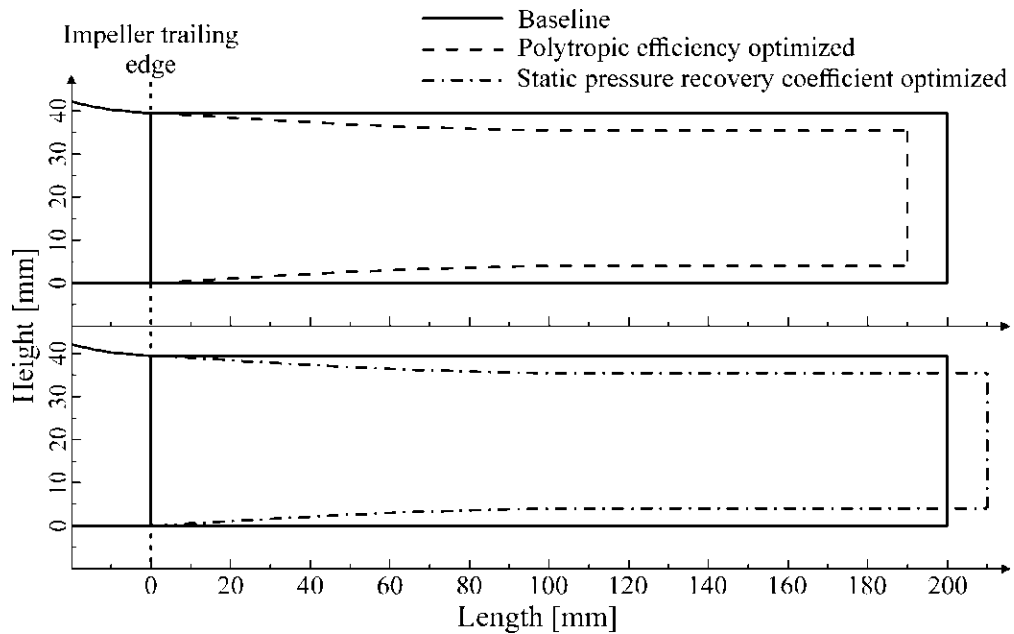
Fig. 34 Optimal parameters for total pressure loss.



Font: Prepared by the author.

The optimal geometry for each objective function in comparison to the baseline can be seen in Fig. 35.

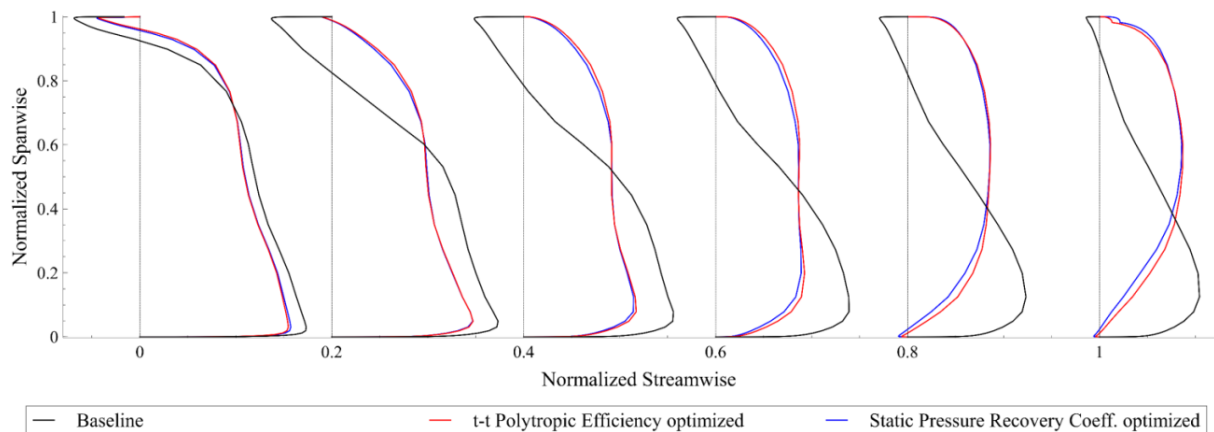
Fig. 35 Meridional shape of vaneless diffuser geometries.



Font: Prepared by the author.

The explanation for such improvements is that the baseline geometry channel showed a recirculation flow close to the shroud, as presented in Fig. 37a, due to the direction of flow at the impeller tip, the pressure gradient due to clearance between blade and shroud and the non-uniformity of the pressure field along the spanwise. Thus, this phenomenon is responsible for accelerating the flow near the hub, increasing the velocity variation along the spanwise in the hub wall and in the vicinity of the recirculation as observed in Fig. 36.

Fig. 36 Behavior of the diffuser meridional velocity along the streamwise.

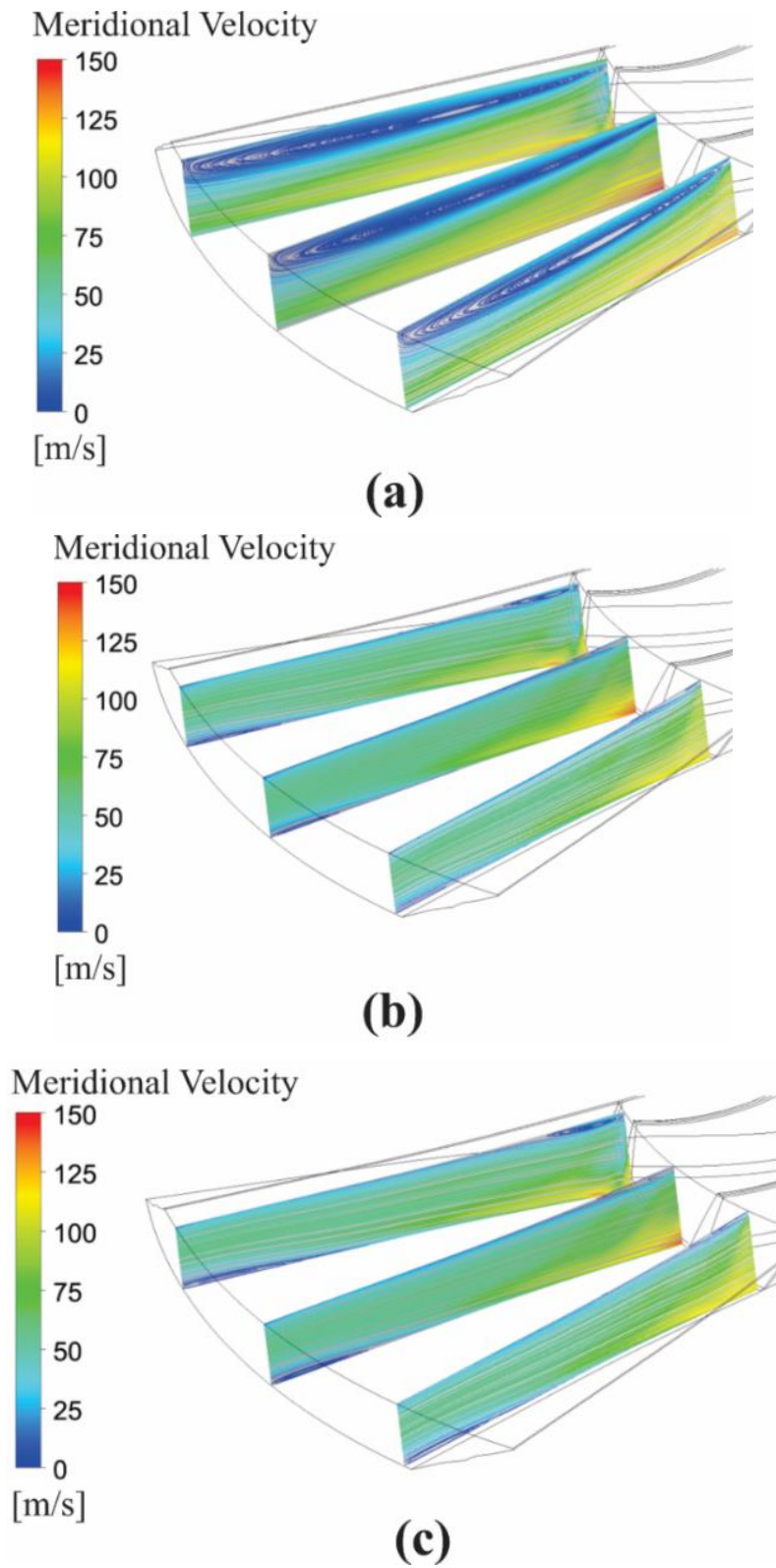


Font: Prepared by the author.

Hence, in these regions, the shear strain rate is significantly high, as seen in Fig. 41a, because such variation is related to friction in viscous flows and, according to Bejan (2016), it is an entropy generation source. Denton (1993) also states that for turbomachinery the recirculation is a loss mechanism not only due to the high shear strain rate values but also due to the wake mixing flow which can be confirmed by viewing the static entropy behavior of baseline geometry along the streamwise in Fig. 38. These mechanisms also impact the total pressure behavior, as can be seen in Fig. 39, since they are closely related to pressure gradient and blockages that cause flow acceleration and pressure variations (DENTON, 1993).

Therefore, the optimization process found a geometry with a narrower channel, shown in Fig. 35, reducing the size of the recirculation region. Such reduction, shown in Fig. 37b and Fig. 37c, improves velocity and total pressure uniformity along the spanwise and decreases the meridional velocity peak and its variation regarding spanwise, as presented in Fig. 36, which decreases the shear strain rate, as can be seen in Fig. 41b and Fig. 41c.

Fig. 37 Streamlines of meridional velocity in (a) baseline, (b) t-t polytropic efficiency optimized and (c) static pressure recovery coefficient optimized geometries.

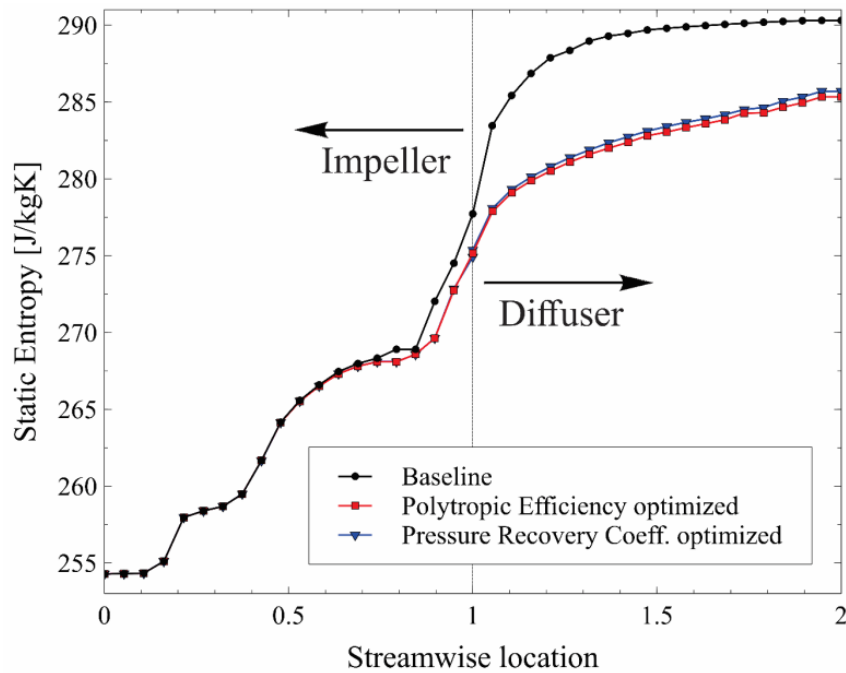


Font: Prepared by the author.

The entropy generation reduction increases available pressure at the impeller outlet, since the loss at the diffuser entrance is smaller, as shown in Fig. 39. Consequently, the total pressure at the outlet for an optimal design is higher than for baseline geometry, i.e., less pressure loss is verified due to reduction in the maximum meridional velocity and its uniformization, contributing to increasing the static pressure recovery, as can be seen in Fig. 40.

Also, as it can be seen in Fig. 38, changes in diffuser geometry impact the entropy generation upstream at the impeller trailing edge and remain to change up to the entrance of the diffuser, which makes the entropy at the outlet of the baseline significantly higher than in the optimal cases. Thus, the polytropic and isentropic efficiency increases, considering its dependence on the variation of such thermodynamic property.

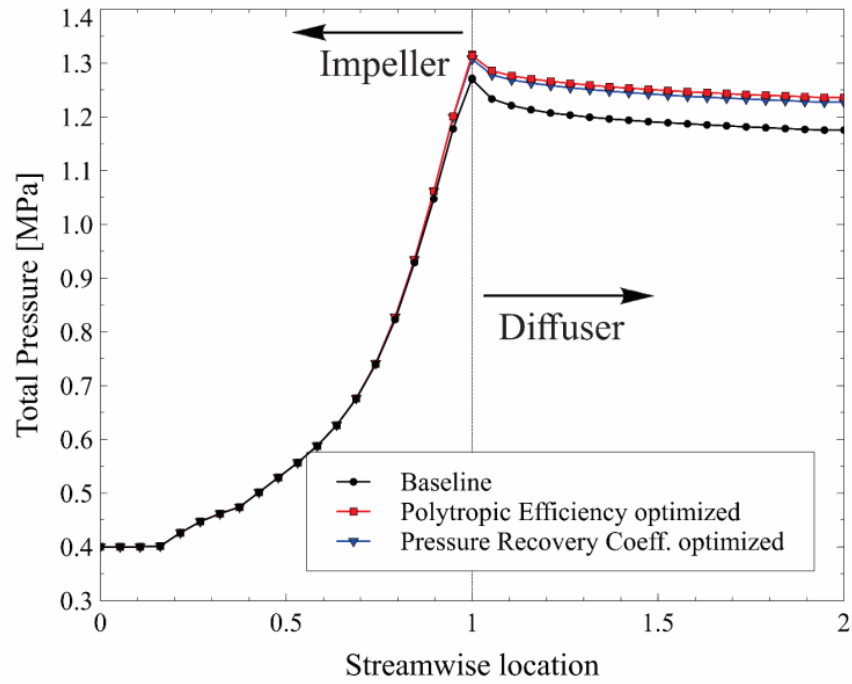
Fig. 38 Entropy as a function of streamwise.



Font: Prepared by the author.

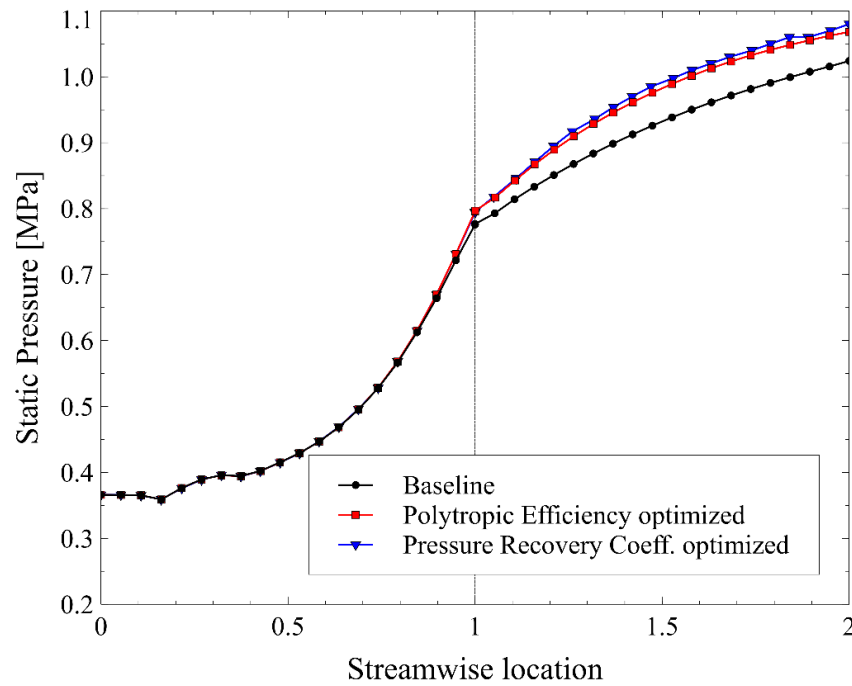
Furthermore, considering these four objective functions, the optimization procedure through response surface trained from the same quasi-optimal sample reduced the computational cost from 14 months to 19 days since each simulation took about 4 hours to run and it would take 2500 cases to reach the convergence of the optimization method (NSGA-II) and just 100 for the RSM method.

Fig. 39 Total pressure as a function of streamwise.



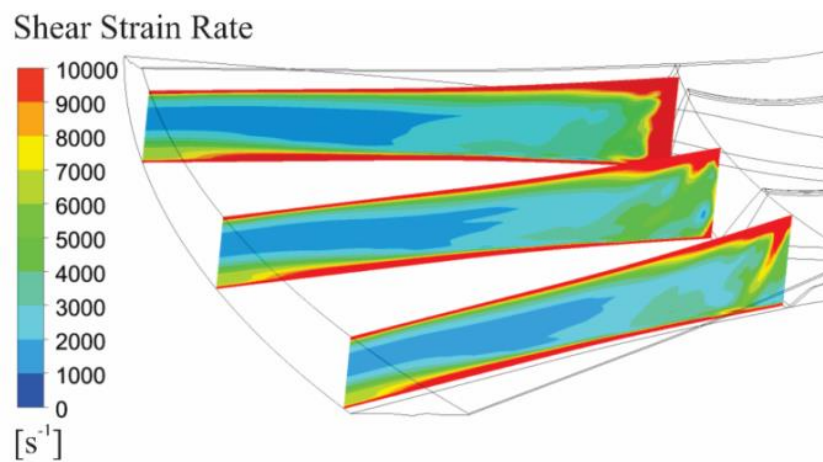
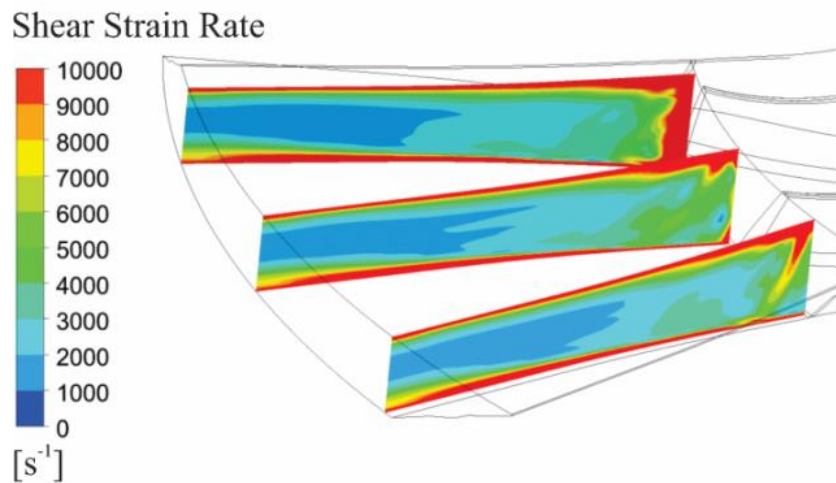
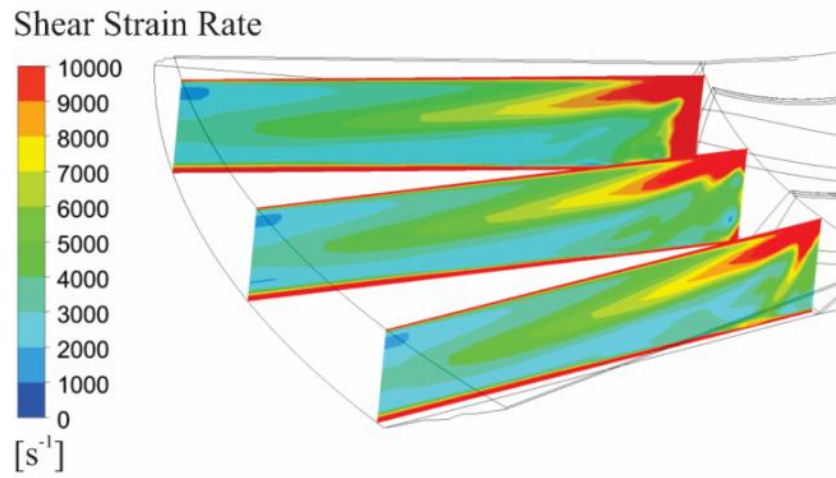
Font: Prepared by the author.

Fig. 40 Static pressure as a function of streamwise.



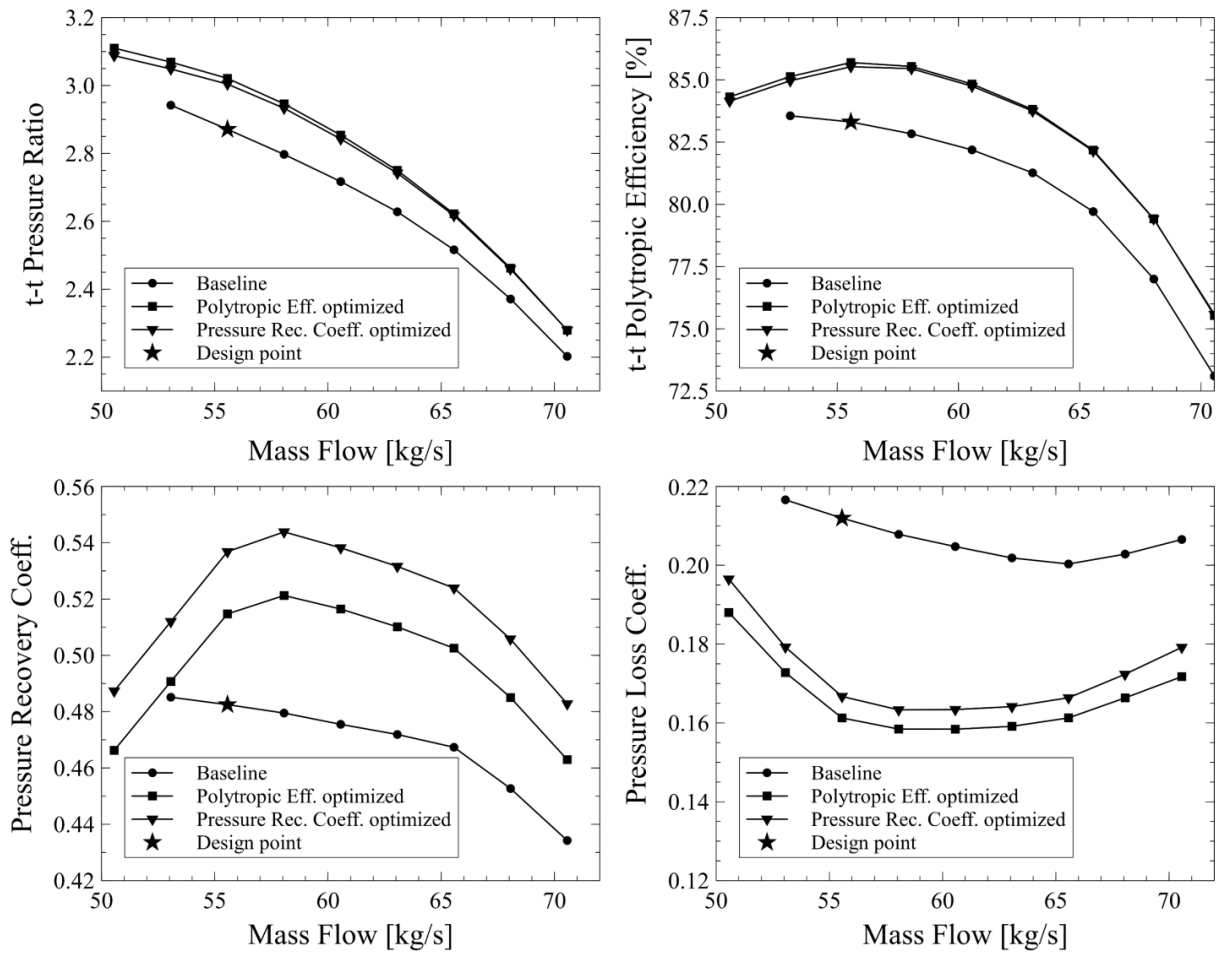
Font: Prepared by the author.

Fig. 41 Shear strain rate contours of (a) baseline geometry, (b) optimal polytropic efficiency and (c) optimal static pressure recovery coefficient.



Font: Prepared by the author.

Fig. 42 Compressor performance in the design Speedline (12.500 RPM).



Font: Prepared by the author.

Fig. 42 shows that all turbomachine performance parameters defined for the present analysis achieved higher values for those optimal cases than for the baseline even for off-design operating points. It ensures the reliability of the centrifugal compressor and the method used in the present work to find the optimal sCO₂ centrifugal compressor design. Moreover, the optimal geometry found for pressure recovery presents efficiency and losses similar to those verified for optimization of the polytropic efficiency. However, the choice of final geometry of the centrifugal compressor depends on the requirements of the project such as available size, static pressure required, velocity limitation and others.

5. CONCLUSIONS

The combined approach through one-dimensional turbomachinery design with three-dimensional parametric sensitivity analysis and CFD-surrogate-optimization of a vaneless-diffusers proved to be a powerful strategy to design a high-efficiency sCO₂ centrifugal compressor since the method found a suitable geometry from a diffuser without prior 1D or 2D design in less than a month of simulations. Also, some highlights are presented:

- Morris method is a robust tool even with only 10 trajectories since there is a small difference of 0.15% in polytropic efficiency, 0.66% in t-t pressure ratio, 0.56% in static pressure recovery coefficient and 3.1% in total pressure loss coefficient considering all input variables or eliminating the non-influential. Results by the Morris method were similar to those found by the SS-ANOVA method;
- The main vaneless-diffuser input variables are S2 and H2 together with S1 and H1 due to the impact caused on flow recirculation of the baseline geometry. The length variable, on the other hand, appears as influential due to the impact on static pressure recovery and total pressure loss by skin friction. Therefore, for increasing efficiency and decreasing pressure loss, the optimization indicated the shortening of the channel to reduce friction area between fluid and wall and to increase the static pressure recovery the optimizer led to the increase of the channel;
- The optimized geometries found achieved an increase of 2.87% for total-to-total polytropic efficiency, a reduction of 24.0% of the total pressure loss coefficient and an increase by 11.4% for static pressure recovery coefficient at the design-point operational condition. Optimal devices not only improved the aerodynamic performance of the centrifugal compressor by increasing the available pressure at the impeller outlet and decreasing losses along the channel, but also an improvement in the transformation of dynamic pressure into static pressure;
- The optimal configuration found by the optimization procedure remains with higher performance even operating at the off-design point;
- Optimal geometry indicated the narrowing of the channel to minimize the recirculation, resulting in higher uniformity of meridional velocity field and reduction of the specific entropy variation along the streamwise, especially at the diffuser inlet, which increases the polytropic efficiency and decreases the intensity

of the total pressure gradient;

- Additionally, increasing the polytropic efficiency and decreasing the total pressure loss coefficient led to the same geometry, similar to claimed by Aungier (2000b) that the polytropic efficiency purely reflects the aerodynamic performance by disregarding the undesirable thermodynamic effects due to pressure ratio differences.

REFERENCES

- ANSYS CFX-Solver Theory Guide**. . Canonsburg, PA: Ansys Inc., 2009.
- AUNGIER, R. H. A Fast, Accurate Real Gas Equation of State for Fluid Dynamic Analysis Applications. **Journal of Fluids Engineering**, v. 117, n. 2, p. 277–281, 1995.
- AUNGIER, R. H. Vaneless Diffuser Design. Em: **Centrifugal Compressors: A Strategy for Aerodynamic Design and Analysis**. 1. ed. New York: ASME Press, 2000a. p. 159–166.
- AUNGIER, R. H. **Centrifugal Compressors: A Strategy for Aerodynamic Design and Analysis**. 1. ed. New York: ASME Press, 2000b.
- AUNGIER, R. H. One-Dimensional Aerodynamic Performance Analysis. Em: **Centrifugal Compressors: A Strategy for Aerodynamic Design and Analysis**. 1. ed. New York: ASME Press, 2000c. p. 69–108.
- AUNGIER, R. H. Thermodynamics. Em: **Centrifugal Compressors: A Strategy for Aerodynamic Design and Analysis**. 1. ed. New York: ASME Press, 2000d. p. 13–34.
- BARTH, T. J.; JESPERSEN, D. C. The Design and Application of Upwind Schemes on Unstructured Meshes. **AIAA**, v. 89, n. 366, p. 1–12, 1989.
- BEJAN, A. Entropy Generation, or Exergy Destruction. Em: **Advanced Engineering Thermodynamics**. 4. ed. Hoboken, New Jersey: John Wiley & Sons, Inc., 2016. p. 101–144.
- BRENES, B. **Design of supercritical carbon dioxide centrifugal compressors**. Seville: [s.n.].
- CAMPOLONGO, F.; CARIBONI, J.; SALTELLI, A. An Effective Screening Design for Sensitivity Analysis of Large Models. **Environmental Modelling and Software**, v. 22, n. 10, p. 1509–1518, out. 2007.
- CASEY, M. V.; ROBINSON, C. J. **A Guide to Turbocharger Compressor Characteristics**. Symposium Dieselmotorentchnik, 10. **Anais...**Ostfildern, Germany: TIB Hannover, 2006.
- CELIK, I. B. et al. Procedure for Estimation and Reporting of Uncertainty Due to Discretization in CFD Applications. **Journal of Fluids Engineering, Transactions of the ASME**, v. 130, n. 7, p. 78001/1–78001/4, 2008.
- DEAN, R. C.; SENOO, Y. Rotating Wakes in Vaneless Diffusers. **Journal of Basic Engineering**, v. 82, n. 3, p. 563–570, 1 set. 1960.
- DEB, K. et al. A fast and elitist multiobjective genetic algorithm: NSGA-II. **IEEE Transactions on Evolutionary Computation**, v. 6, n. 2, p. 182–197, abr. 2002.

- DEB, K. **Multi-Objective Optimization Using Evolutionary Algorithms: An Introduction**. [s.l.: s.n.]. Disponível em: <<http://www.iitk.ac.in/kangal/deb.htm>>.
- DENTON, J. D. Loss Mechanisms in Turbomachines. **Journal of Turbomachinery**, v. 115, n. 4, p. 621–656, 1 out. 1993.
- ECKARDT, D. Instantaneous Measurements in the Jet-Wake Discharge Flow of a Centrifugal Compressor Impeller. **Journal of Engineering for Power**, v. 97, n. 3, p. 337–345, 1 jul. 1975.
- FORRESTER, A. I. J.; SÓBESTER, A.; KEANE, A. J. **Engineering Design via Surrogate Modelling: A Practical Guide**. [s.l.] John Wiley & Sons Ltd., 2008.
- GE, Q.; CIUFFO, B.; MENENDEZ, M. Combining screening and metamodel-based methods: An efficient sequential approach for the sensitivity analysis of model outputs. **Reliability Engineering and System Safety**, v. 134, n. 2015, p. 334–344, 2015.
- GODEC, M. et al. **CO₂ storage in depleted oil fields: The worldwide potential for carbon dioxide enhanced oil recovery**. Energy Procedia. Anais...Elsevier Ltd, 2011.
- GU, C. **Smoothing Spline ANOVA Models**. 2. ed. New York: Springer Series in Statistics, 2013. v. 297
- HEINRICH, M. **Genetic Optimization of Turbomachinery Components using the Volute of a Transonic Centrifugal Compressor as a Case Study**. Freiberg: American Society of Mechanical Engineers (ASME), 22 nov. 2016.
- HE, X.; ZHENG, X. Performance Improvement of Transonic Centrifugal Compressors by Optimization of Complex Three-Dimensional Features. **Proceedings of the Institution of Mechanical Engineers, Part G: Journal of Aerospace Engineering**, v. 231, n. 14, p. 2723–2738, 1 dez. 2017.
- JAATINEN, A. **Performance improvement of centrifugal compressor stage with pinched geometry or vaned diffuser**. [s.l.] Lappeenranta Teknillinen Yliopisto, 2009.
- KIM, J. H. et al. Multi-objective optimization of a centrifugal compressor impeller through evolutionary algorithms. **Proceedings of the Institution of Mechanical Engineers, Part A: Journal of Power and Energy**, v. 224, n. 5, p. 711–721, 1 jan. 2010.
- KRAIN, H. A Study on Centrifugal Impeller and Diffuser Flow. **Journal of Engineering for Power**, v. 103, n. 4, p. 688–697, 1981.
- LEE, Y. T.; LUO, L.; BEIN, T. W. Direct method for optimization of a centrifugal compressor vaneless diffuser. **Proceedings of the ASME Turbo Expo**, v. 1, p. 73–80, 2000.

- MAJUMDAR, S.; RODI, W.; ZHU, J. Three-Dimensional Finite-Volume Method for Incompressible Flows With Complex Boundaries. **Journal of Fluids Engineering**, v. 114, p. 496–503, 1992.
- MALLEN, M.; SAVILLE, G. **Polytropic Processes in the Performance Prediction of Centrifugal Compressors**. Scaling for performance prediction in rotodynamic machines: a conference held at the University of Stirling. **Anais...**London: Institution of Mechanical Engineers, 1977.
- MATTOS, V. C. N. et al. **Sensitivity Analysis Based on Morris Screening Method for Blade Design of a Centrifugal Compressor**. Proceedings of the Ibero-Latin-American Congress on Computational Methods in Engineering. **Anais...**Natal-RN: ABMEC, 2019.
- MCKAY, M. D.; BECKMAN, R. J.; CONOVER, W. J. A Comparison of Three Methods for Selecting Values of Input Variables in the Analysis of Output from a Computer Code. **Technometrics - American Statistical Association**, v. 21, n. 2, p. 239–245, 1979.
- MENTER, F. R. Two-equation eddy-viscosity turbulence models for engineering applications. **AIAA Journal**, v. 32, n. 8, p. 1598–1605, 1994.
- MOJADDAM, M.; PULLEN, K. R. Optimization of a Centrifugal Compressor Using the Design of Experiment technique. **Applied Sciences**, v. 9, n. 291, p. 1–20, 15 jan. 2019.
- MORRIS, M. D. Factorial Sampling Plans for Preliminary Computational Experiments. **Technometrics**, v. 33, n. 2, p. 161–174, 1991.
- PINARBASI, A.; JOHNSON, M. W. Off-Design Flow Measurements in a Centrifugal Compressor Vaneless Diffuser. **Journal of Turbomachinery**, v. 117, n. 4, p. 602–608, 1 out. 1995.
- RHIE, C. M.; CHOW, W. L. Numerical study of the turbulent flow past an airfoil with trailing edge separation. **AIAA Journal**, v. 21, n. 11, p. 1525–1532, 1983.
- SALTELLI, A. et al. Elementary Effects Method. Em: **Global Sensitivity Analysis. The Primer**. 1. ed. Chichester, UK: John Wiley & Sons, Ltd, 2007. p. 109–154.
- SALVIANO, L. O. et al. Sensitivity analysis and optimization of a CO₂ centrifugal compressor impeller with a vaneless diffuser. **Structural and Multidisciplinary Optimization**, v. 64, n. 3, p. 1607–1627, 2021.
- SEGURA, C.; SEGREDO, E.; LEÓN, C. Analysing the Robustness of Multiobjectivisation Approaches Applied to Large Scale Optimisation Problems. Em: **A Bridge between Probability, Set Oriented Numerics and Evolutionary Computation. Studies in Computational Intelligence**. Berlin, Heidelberg: Springer, 2013. v. 447p. 365–391.

SHAABAN, S. Design Optimization of a Centrifugal Compressor Vaneless Diffuser. **International Journal of Refrigeration**, v. 60, p. 142–154, dez. 2015.

SUGIMURA, K.; KOBAYASHI, H.; NISHIDA, H. **Design Optimization and Experimental Verification of Centrifugal Compressors with Curvilinear Element Blades**. Proceedings of ASME Turbo Expo 2012. **Anais...2012**. Disponível em: <<http://www.asme.org/about-asme/terms-of-use>>

Technology Assessments. Em: **Quadrennial Technology Review**. [s.l.] U.S. Department of Energy, 2015. p. 1–28.

TURUNEN-SAARESTI, T. **Computational and Experimental Analysis of Flow Field in the Diffusers of Centrifugal Compressors**. Lappeenranta, Finland: [s.n.].

VANROLLEGHEM, P. A. et al. Global sensitivity analysis for urban water quality modeling: Terminology, convergence and comparison of different methods. **Journal of Hydrology**, v. 522, n. 2015, p. 339–352, 2015.

WRIGHT, S. et al. **Operation and analysis of a supercritical CO₂ Brayton cycle**. Albuquerque, NM, and Livermore, CA (United States): [s.n.]. Disponível em: <<https://www.osti.gov/servlets/purl/984129/>>.